Computer Methods in Applied Mechanics and Engineering 418 (2024) 116556

Contents lists available at ScienceDirect

Comput. Methods Appl. Mech. Engrg.

journal homepage: www.elsevier.com/locate/cma

Large deformation Kirchhoff–Love shell hierarchically enriched with warping: Isogeometric formulation and modeling of alternating stiff/soft layups

Domenico Magisano [a,*], Antonella Corrado [a], Leonardo Leonetti [a], Josef Kiendl [b], Giovanni Garcea [a]

[a] Department of Computer Science, Modeling, Electronics and Systems Engineering, University of Calabria, 87030, Rende (Cosenza), Italy
[b] Institute of Engineering Mechanics and Structural Analysis, Bundeswehr University Munich, Werner-Heisenberg-Weg 39, 85577 Neubiberg, Germany

ARTICLE INFO

Keywords:
Composite shells
Warping
Large deformation
Buckling
Isogeometric analysis

ABSTRACT

This paper presents a large deformation Kirchhoff–Love shell model hierarchically enhanced with through-the-thickness warping functions, arbitrarily chosen by the user. Two unknowns are introduced for each of them, representing its amplitudes in two directions tangent to the shell surface. NURBS are used to approximate reference surface displacement and warping amplitudes in the weak form. The transverse shear strains are linear functions of the warping parameters only and naturally free from locking. A patch-wise reduced integration avoids membrane locking and improves efficiency. Particular attention is paid to the modeling of composites made up of multiple stiff layers coupled with soft interlayers. The alternating layup with high stiffness ratios induces a significant sectional warping with transverse shear strains concentrated in the soft layers. Two warping models are investigated: (WI) all stiff layers maintain the same director orthogonal to the deformed surface with independent transverse shear deformations of the soft layers; (WZ) a single zigzag function linking these deformations. The numerical tests confirm the great accuracy of the hierarchic shell model in reproducing the solid solution with a small number of discrete parameters, provided that the correct warping model is chosen. WI is reliable for all alternating layups. WZ reduces the unknowns to five per surface point, regardless of the number of layers, and is accurate for uniform soft layers.

1. Introduction

The use of composite materials, thanks to their properties of strength and lightness, has opened new horizons in various engineering fields. Laminated composites are obtained by a piling of layers of different materials, or of plies of the same material but with different orientation, as in fiber-reinforced composites. The non-uniform distribution of the material properties over the thickness direction accentuates a certain deformation phenomenology: transverse shear strains become important and the planarity of the deformed section is often lost even for rather slender structures. Each layer may exhibit a different angle of rotation and the final configuration of the deformed cross-section assumes a zigzag shape, that is a piece-wise linear configuration. Although the application of these materials is now widespread, the development of accurate and affordable analysis and design methods is still an

* Corresponding author.
E-mail addresses: domenico.magisano@unical.it (D. Magisano), antonella.corrado@unical.it (A. Corrado), leonardo.leonetti@unical.it (L. Leonetti), josef.kiendl@unibw.de (J. Kiendl), giovanni.garcea@unical.it (G. Garcea).

https://doi.org/10.1016/j.cma.2023.116556
Received 27 May 2023; Received in revised form 12 October 2023; Accepted 17 October 2023
Available online 26 October 2023

open topic in the scientific community, in particular because the layup configuration influences significantly the modeling rules. The use of a fully 3D model with a finite element discretization through the laminate thickness, despite being the most versatile, requires computational resources usually not affordable in the design stage, especially if nonlinear analyses are needed. Often, it is restricted to the analysis of some small portions of interest [1], coupling the analysis with a two-dimensional discretization. Concerning plate/shell models, two main approaches are usually followed: the equivalent single-layer theories (ESL) and the layer-wise theories (LW).

Within the framework of the ESL models, the easiest approach followed in the early studies is the classical Kirchhoff–Love theory of the plates. Based on the assumptions of neglecting the transverse shear effects, this proved to be reliable only for very slender structures. Moreover, it was employed mainly for analytical solutions for simple geometries, due to the C^1 continuity requirement of the weak form, until the spread of spline-based (e.g. [2–4]) and other novel discretization strategies [5]. Finite elements based on the First Order Shear Deformation Theory (FSDT) are widely used to include the transverse shear deformations and they were the natural progress in modeling composite laminates. However, the hypothesis of cross-sections remaining planar after deformation restricts the capacity of this model, which does not take into account the cross-sectional warping becoming more and more important as the stiffness ratios of the different layers grow. In High Order Shear Deformation (HSDT) Theories the in-plane displacement description is enriched with higher-order terms of the thickness coordinate [6] in order to include warping. However, even in this case, the cross-sectional zigzag warping affecting some types of laminates is not represented accurately unless many higher-order terms are used so affecting the computational burden. Halfway between FSDT and HSDT, we can find a recent proposal [7], where the Mindlin–Reissner model is extended with an element-wise displacement fluctuation describing warping and thickness changes, whose associated DOFs can be condensed out to maintain the usual 5 or 6 DOFs per node at the global level.

The Zigzag Theory (ZZT) represents the attempt to take into account the cross-sectional warping keeping the framework of the ESL approaches. In ZZT [8–10] a piece-wise linear zigzag-shaped contribution is added to the in-plane displacements employing the first order, or higher order, shear deformation theories *at each layer* and imposing continuity conditions at the interfaces. Compared to the FSDT theory, one unknown for each in-plane direction is added, which represent the amplitude of the zigzag functions, keeping the number of unknowns independent from the number of layers. Among the ZZTs, the Refined ZZT [11–13] is one of the most used approaches. Clearly, the accuracy of this approach depends on how well the assigned zigzag function approximates the actual warping.

The LW theories [14–17] have a quasi-3D description capability, since the displacement is approximated within each layer. The displacement field is continuous over the thickness but the derivatives with respect to the thickness coordinate are not. This means that the strains are discontinuous at the layer interfaces and there is the possibility for the inter-laminar transverse stresses computed from the constitutive relations to be continuous. Opposite considerations can be made for the in-plane strains and stresses [6]. The main drawback of LW theories is that the number of unknowns depends on the number of layers and can become prohibitive in some applications. Recent advances in LW approaches model each lamina as a Kirchhoff–Love thin shell with a spline-based discretization and a focus on the modeling of damage [18–20].

In short, the efficiency of a model for composite laminates can be assumed mainly as a function of the number of independent variables. The accuracy, instead, is related to the ability to reproduce the warping over the thickness and, in particular the zigzag deformation. An important point to take into account is that, although many of the discussed models were developed and validated in the small deformation case, the slenderness of most composite structures is likely to induce large deflections and/or buckling. This means that a geometrically nonlinear analysis is usually necessary. There exists a number of large deformation models for composite structures, many of them reusing the small deformation models by means of hierarchic [21] or co-rotational strategies [22].

Besides shell models, it is worth mentioning the solid-shell approach [23–25], based on a large deformation 3D continuum model with a linear kinematic approximation through-the-thickness and only displacement DOFs. For laminates, homogenized solid-shell models (ESL) equivalent to the first order shear deformation theory are presented in [23]. One element per layer can be also adopted when needed to model the sectional warping (LW). In this last case, the model goes in the direction of the so-called multi-director concept [26,27].

Multi-layered composite shells made of a number of stiff plies shear-coupled by soft interlayers are a typical case of laminates whose mechanics is dominated by the zigzag effects. Among many others, typical examples are represented by laminated glass and metal-polymer laminates, i.e. glass or metal plies bonded by polymeric interlayers. Although the soft interlayers have in practice no bending stiffness by themselves, they can restrain the shear-sliding of the stiff plies increasing the overall bending capacity of the laminate [28], which varies [29] between the lower bound of free-sliding stiff plies (layered limit) and the upper-bound of perfectly coupled plies (monolithic limit). The alternating layup induces a specific straining/deformation pattern, which distinguishes them from other composites [22,30]. In fact, the transverse shear strains tend to concentrate in the soft interlayers, with a nearly constant distribution in the thickness, while they are negligible in the stiff plies. Moreover, although the interlayers are soft, they constrain the relative distance between the surfaces to which they adhere. The consequence is that the stiff layers are all subjected to almost identical rotations with respect with their normals in the initial configuration, while the soft layers undergo independent transverse shear strains. Different plate/shell models have been proposed for alternating layups. A reference paper in the field is [22] where, for the first time, a shell model imposing equal rotation of the stiff layers and independent shear deformations of the soft interlayers was proposed. This is a Mindlin–Reissner model enriched by independent in-plane displacements of the soft layers. The same work implements a locking-free shell finite element with the geometrically nonlinear model recovered by the co-rotational approach [31]. The kinematics with independent shear deformations of the soft layers [22] results useful also for including thermal and viscous effects [32] and for modeling more general boundary conditions. Most often, the stiff layers tend to exhibit negligible transverse shear strains. Although limited to small-displacement analyses, the Kirchhoff–Love assumption of neglecting the transverse shear

strains in the stiff layers was exploited in [30], with the aim of further reducing the model variables. The C^1 continuity requirement is met with special finite elements. In [21] a hierarchic implementation of the Refined ZZT [11–13] is proposed, adopting finite elements based on the geometrically exact shell theory of Simo [33], in order to economically describe the behavior of composite laminates undergoing large deformations but small strains by adding only two additional DOFs. A linear finite element approximation of geometry and kinematics is considered in this work.

In [34], a nonlinear KL model is extended hierarchically with linearized transverse shear components. Two formulations are proposed, using hierarchic rotations or hierarchic displacement to include the transverse shear effects. The basic assumption, confirmed by numerical investigation, is that the transverse shear strains remain small in most simulations involving large deflections.

Inspired by this work, this paper proposes a large deformation/small strain Kirchhoff–Love shell model hierarchically enhanced with warping. The warping displacement is additional with respect to the arbitrarily large displacement of the shell reference surface. Hence, it is purely deformational, i.e. not affected by rigid body motions, and small allowing an additive split of the strain into the nonlinear part of the basic Kirchhoff–Love model and a linear part of the additional warping deformation. The resulting model is geometrically exact, in the sense that the overall strain measure is not influenced by arbitrarily large rigid motions. Warping is described as combination of a number of through-the-thickness shape functions, generically selected by the user. Two unknowns are introduced for each warping shape, representing its amplitudes in two directions tangent to the shell surface. The plane stress condition is exploited as usual. In the framework of the isogeometric analysis, NURBS basis functions are used to approximate reference surface displacement and warping amplitudes, in order to meet the continuity requirement of the weak form. The transverse shear strains depend only on the warping amplitudes. They are linear with the corresponding DOFs and naturally free from locking. Membrane locking is avoided by a proper choice of the basis functions degree and the adoption of an efficient patch-wise reduced integration scheme for the strain energy associated to the in-plane strain components, the only integration to be repeated in the nonlinear analysis. Particular focus is given to the modeling of composite plates and shells with alternating stiff/soft layups, for which two warping models are investigated. The first one assumes that all stiff layers maintain the same director orthogonal to the deformed surface with independent transverse shear deformations of the soft layers. This can be considered as an exact geometry, Total-Lagrangian, rotation-free, higher order version of the proposal in [22], that exploits the negligible transverse shear deformations of the stiff layers to reduce the number of variables per surface point. A second model uses a single zigzag function linking the transverse shear deformations of the soft layers to further reduce the variables to five per surface point, regardless of the number of layers. A set of numerical tests is reported to assess the validity of the hierarchic formulation and the coarse-mesh accuracy of the discretization. In addition, a critical evaluation of the reliability of the two warping models compared to the solid solution is carried out, showing in which cases one model is preferable to the other.

The article is organized as follows. After a brief introduction to the Kirchhoff–Love shell model, Section 2 formulates the Kirchhoff–Love model hierarchically enhanced with generic warping functions in a large deformation/small strain context. Warping models for laminates with alternating stiff/soft layups are presented in Section 3. Details concerning the isogeometric discretization and the nonlinear analysis are reported in Section 4. Section 5 contains a significant set of numerical tests. Conclusions are drawn in Section 6.

2. Hierarchic Kirchhoff–Love shell model with warping

2.1. Standard Kirchhoff–Love shell

A set of convective coordinates ξ^α, with $\alpha = 1,2$ is considered over a suitable reference shell surface (not necessarily being the middle surface of the shell), while in the thickness direction the coordinate $\xi^3 \in [\xi^3_b, \xi^3_t]$ is assumed with ξ^3_b and ξ^3_t identifying the offset of bottom and top surfaces of the body with respect to the reference one. The position of a point in the undeformed configuration is defined by the position vector $\mathbf{X}$

$$\mathbf{X} = \mathbf{R}(\xi^1, \xi^2) + \xi^3 \mathbf{A}_3(\xi^1, \xi^2) \tag{1}$$

where $\mathbf{R}(\xi^1, \xi^2)$ represents the position of the corresponding point on the reference surface and $\mathbf{A}_3$ the initial shell normal taken as

$$\mathbf{A}_3 = \frac{\mathbf{A}_1 \times \mathbf{A}_2}{|\mathbf{A}_1 \times \mathbf{A}_2|}. \tag{2}$$

with vectors

$$\mathbf{A}_\alpha = \frac{\partial \mathbf{R}}{\partial \xi^\alpha} \qquad \text{with} \quad \alpha = 1,2$$

defining a tangent plane to the shell surface. Covariant base vectors $\mathbf{G}_\alpha$ in the reference configuration can be then evaluated as

$$\begin{aligned} \mathbf{G}_\alpha &= \frac{\partial \mathbf{X}}{\partial \xi^\alpha} = \mathbf{A}_\alpha + \xi^3 \mathbf{A}_{3,\alpha} \qquad \text{with} \quad \alpha = 1,2 \\ \mathbf{G}_3 &= \frac{\partial \mathbf{X}}{\partial \xi^3} = \mathbf{A}_3 \end{aligned} \tag{3}$$

The current deformed configuration is described as

$$\mathbf{x} = \mathbf{r}(\xi^1, \xi^2) + \xi^3 \mathbf{a}_3(\xi^1, \xi^2) \tag{4}$$

where $\mathbf{r} = \mathbf{R} + \mathbf{v}$ is the current position of the reference surface, with $\mathbf{v}$ its displacement. Introducing the reference surface covariant basis vectors in the deformed configuration

$$\mathbf{a}_\alpha = \frac{\partial \mathbf{r}}{\partial \xi_\alpha} = \mathbf{A}_\alpha + \mathbf{v}_{,\alpha} \qquad \text{with} \quad \alpha = 1,2$$

the current normal is defined as

$$\mathbf{a}_3 = \frac{\mathbf{a}_1 \times \mathbf{a}_2}{|\mathbf{a}_1 \times \mathbf{a}_2|}, \tag{5}$$

according to the Kirchhoff–Love shell assumption that the director remains straight and normal to the shell surface during deformation. The covariant basis vectors in the deformed configuration can be computed over the body as

$$\begin{aligned} \mathbf{g}_\alpha &= \frac{\partial \mathbf{x}}{\partial \xi^\alpha} = \mathbf{a}_\alpha + \xi^3 \mathbf{a}_{3,\alpha} \qquad \text{with} \quad \alpha = 1,2 \\ \mathbf{g}_3 &= \frac{\partial \mathbf{x}}{\partial \xi^3} = \mathbf{a}_3(\xi^1, \xi^2) \end{aligned} \tag{6}$$

Denoting the displacement of the body with

$$\mathbf{u} = \mathbf{x} - \mathbf{X} = \mathbf{v}(\xi^1, \xi^2) + \xi^3(\mathbf{a}_3(\xi^1, \xi^2) - \mathbf{A}_3(\xi^1, \xi^2)) \tag{7}$$

the Green–Lagrange strain tensor can be written as

$$\mathbf{E} = \sum_{i,j=1}^{3} \bar{E}_{ij} \mathbf{G}^i \otimes \mathbf{G}^j \quad \text{with} \quad \bar{E}_{ij} = \frac{1}{2}\left(\mathbf{g}_i \cdot \mathbf{g}_j - \mathbf{G}_i \cdot \mathbf{G}_j\right) = \frac{1}{2}\left(\mathbf{u}_{,i} \cdot \mathbf{G}_j + \mathbf{u}_{,j} \cdot \mathbf{G}_i + \mathbf{u}_{,i} \cdot \mathbf{u}_{,j}\right) \tag{8}$$

where $\bar{E}_{ij}$ are the covariant strain components. The partial derivatives of the displacement vector are

$$\begin{aligned} \mathbf{u}_{,\alpha} &= \mathbf{v}_{,\alpha} + \xi^3(\mathbf{a}_{3,\alpha} - \mathbf{A}_{3,\alpha}) \qquad \text{with} \quad \alpha = 1,2 \\ \mathbf{u}_{,3} &= \mathbf{a}_3(\xi^1, \xi^2) - \mathbf{A}_3(\xi^1, \xi^2) \end{aligned} \tag{9}$$

The reference surface and body contravariant basis vectors are obtained from the dual basis condition $\mathbf{a}_\alpha \cdot \mathbf{a}^\beta = \mathbf{A}_\alpha \cdot \mathbf{A}^\beta = \delta_\alpha^\beta$ and $\mathbf{g}_\alpha \cdot \mathbf{g}^\beta = \mathbf{G}_\alpha \cdot \mathbf{G}^\beta = \delta_\alpha^\beta$, with $\alpha, \beta = 1,2$. Due to Eq. (2) and (5), the transverse shear strains vanish, that is $\bar{E}_{\alpha 3} = 0, \quad \alpha = 1,2$. The same holds for the thickness strain, i.e. $\bar{E}_{33} = 0$. Assuming its components to vary linearly through the thickness, it is possible to separate the strain into a constant part due to membrane action and a linear part due to bending. The covariant strain coefficients are:

$$\bar{E}_{\alpha\beta} = \bar{e}_{\alpha\beta} + \xi^3 \bar{\chi}_{\alpha\beta} = \frac{1}{2}(a_{\alpha\beta} - A_{\alpha\beta}) + \xi^3(B_{\alpha\beta} - b_{\alpha\beta}) \quad \text{with} \quad \alpha, \beta = 1,2 \tag{10}$$

with the metric coefficients $a_{\alpha\beta} = \mathbf{a}_\alpha \cdot \mathbf{a}_\beta$ and $A_{\alpha\beta} = \mathbf{A}_\alpha \cdot \mathbf{A}_\beta$ with $\alpha, \beta = 1,2$. The curvature tensor coefficients [35] are defined as

$$\begin{aligned} B_{\alpha\beta} &= -\frac{1}{2}(\mathbf{A}_\alpha \cdot \mathbf{A}_{3,j} + \mathbf{A}_\beta \cdot \mathbf{A}_{3,\alpha}) = \mathbf{A}_{\alpha,\beta} \cdot \mathbf{A}_3 \\ b_{\alpha\beta} &= -\frac{1}{2}(\mathbf{a}_\alpha \cdot \mathbf{a}_{3,j} + \mathbf{a}_\beta \cdot \mathbf{a}_{3,\alpha}) = \mathbf{a}_{\alpha,\beta} \cdot \mathbf{a}_3 \end{aligned} \tag{11}$$

The curvature components for the Kirchhoff–Love shell can be then computed as

$$\bar{\chi}_{\alpha\beta} = B_{\alpha\beta} - b_{\alpha\beta} = \mathbf{A}_{\alpha,\beta} \cdot \mathbf{A}_3 - \mathbf{a}_{\alpha,\beta} \cdot \mathbf{a}_3 \quad \text{with} \quad \alpha, \beta = 1,2$$

The presence of the norm $|\mathbf{a}_1 \times \mathbf{a}_2|$ in the denominator of $\mathbf{a}_3$ leads to a rather complicated expression of the curvature in terms of the displacement field and, then, a computationally expensive evaluation of the discrete operators coming from the strain variations. A simplified formula for the curvature proposed in [3] is here adopted, exploiting the hypothesis of large deformations but small membrane strains. It is based on the following simplification in Eq. (5):

$$|\mathbf{a}_1 \times \mathbf{a}_2| \approx |\mathbf{A}_1 \times \mathbf{A}_2|.$$

Consequently, $b_{\alpha\beta}$ is simplified as

$$b_{\alpha\beta} \approx \mathbf{a}_{\alpha,\beta} \cdot \frac{\mathbf{a}_1 \times \mathbf{a}_2}{|\mathbf{A}_1 \times \mathbf{A}_2|}.$$

and the curvature components reduce to

$$\bar{\chi}_{\alpha\beta} = B_{\alpha\beta} - b_{\alpha\beta} \approx \frac{1}{|\mathbf{A}_1 \times \mathbf{A}_2|}(\mathbf{A}_{\alpha,\beta} \cdot (\mathbf{A}_1 \times \mathbf{A}_2) - \mathbf{a}_{\alpha,\beta} \cdot (\mathbf{a}_1 \times \mathbf{a}_2)) \quad \alpha, \beta = 1,2 \tag{12}$$

that is a third order dependence on the displacement. The in-plane strain components of the KL model can be written in Voigt's notation as

$$\bar{\boldsymbol{\varepsilon}}_p = \bar{\mathbf{e}} + \xi^3 \bar{\boldsymbol{\chi}} \quad \text{with} \quad \bar{\boldsymbol{\varepsilon}}_p = \begin{bmatrix} \bar{E}_{11} \\ \bar{E}_{22} \\ 2\bar{E}_{12} \end{bmatrix}, \quad \bar{\mathbf{e}} = \begin{bmatrix} \bar{e}_{11} \\ \bar{e}_{22} \\ 2\bar{e}_{12} \end{bmatrix}, \quad \bar{\boldsymbol{\chi}} = \begin{bmatrix} \bar{\chi}_{11} \\ \bar{\chi}_{22} \\ 2\bar{\chi}_{12} \end{bmatrix}. \tag{13}$$

2.2. Hierarchic shell model with warping

Multiple warping deformations, assumed to be small, can be hierarchically added to the KL shell kinematics. Let us consider the case of an overall warping profile expressed as a combination of n shapes $w_k(\xi^3)$. The current configuration is defined as:

$$\mathbf{x} = \mathbf{r}(\xi^1,\xi^2) + \xi^3\mathbf{a}_3(\xi^1,\xi^2) + \sum_{k=1}^{n}\sum_{\beta=1}^{2}\mu_{\beta k}(\xi^1,\xi^2)w_k(\xi^3)\mathbf{a}_\beta(\xi_1,\xi_2) \tag{14}$$

where $\mu_{\beta k}(\xi^1,\xi^2)$ represents the amplitude of the kth warping shape directed along the surface tangent vectors $\mathbf{a}_\beta$ with $\beta = 1,2$ respectively. The profile is assumed to be approximated by the same shapes (with different amplitudes) along the 2 directions, as typical for example for composites made of isotropic layers, also if the generalization to different shapes could be considered for generic composites [21]. The covariant base vectors are defined as:

$$\begin{aligned}
\mathbf{g}_\alpha &= \frac{\partial\mathbf{x}}{\partial\xi^\alpha} = \mathbf{a}_\alpha + \xi^3\mathbf{a}_{3,\alpha} + \sum_{k=1}^{n}\sum_{\beta=1}^{2}\left(\mu_{\beta k}(\xi^1,\xi^2)w_k(\xi^3)\mathbf{a}_{\beta,\alpha} + \mu_{\beta k,\alpha}\,w_k(\xi^3)\mathbf{a}_\beta\right), \quad \alpha = 1,2\\
\mathbf{g}_3 &= \frac{\partial\mathbf{x}}{\partial\xi^3} = \mathbf{a}_3(\xi^1,\xi^2) + \sum_{k=1}^{n}\sum_{\beta=1}^{2}\mu_{\beta k}w_{k,3}\,\mathbf{a}_\beta(\xi_1,\xi_2)
\end{aligned} \tag{15}$$

Using (14) and (1), the displacement field assumes the expression:

$$\mathbf{u} = \mathbf{x} - \mathbf{X} = \underbrace{\mathbf{v}(\xi^1,\xi^2) + \xi^3(\mathbf{a}_3(\xi^1,\xi^2) - \mathbf{A}_3(\xi^1,\xi^2))}_{\mathbf{u}^{KL}} + \underbrace{\sum_{k=1}^{n}\sum_{\beta=1}^{2}\mu_{\beta k}w_k(\xi^3)\mathbf{a}_\beta(\xi_1,\xi_2)}_{\mathbf{u}^{Z}} \tag{16}$$

where $\mathbf{u}^{KL}$ represents the displacement coming from the KL model and $\mathbf{u}^{Z}$ is the contribution given by warping. Analogously, the derivatives of the displacements can be expressed as the sum of the KL and warping contributions:

$$\begin{aligned}
\mathbf{u}_{,\alpha} &= \mathbf{u}^{KL}_{,\alpha} + \mathbf{u}^{Z}_{,\alpha} \quad \text{with} \quad \mathbf{u}^{Z}_{,\alpha} = \sum_{k=1}^{n}\sum_{\beta=1}^{2}(\mu_{\beta k}\mathbf{a}_{\beta,\alpha} + \mu_{\beta k,\alpha}\,\mathbf{a}_\beta)w_k, \quad \alpha = 1,2\\
\mathbf{u}_{,3} &= \mathbf{u}^{KL}_{,3} + \mathbf{u}^{Z}_{,3} \quad \text{with} \quad \mathbf{u}^{Z}_{,3} = \sum_{k=1}^{n}\sum_{\beta=1}^{2}\mu_{\beta k}\mathbf{a}_\beta w_{k,3}
\end{aligned} \tag{17}$$

The covariant strain components can be linearized with respect to the warping amplitudes, collected in vector $\boldsymbol{\mu}$, as

$$\bar{E}_{ij} = \underbrace{\left[\bar{E}_{ij}\right]_{\boldsymbol{\mu}=\mathbf{0}}}_{\bar{E}^{KL}_{ij}} + \underbrace{\left[\frac{\partial\bar{E}_{ij}}{\partial\boldsymbol{\mu}}\right]_{\boldsymbol{\mu}=\mathbf{0}}\cdot\boldsymbol{\mu}}_{\bar{E}^{Z}_{ij}}, \quad \text{with} \quad i,j = 1,2,3 \tag{18}$$

and, neglecting terms more than linear in ξ^3 and w_α, the additional warping contribution to the strain is

$$\begin{aligned}
\bar{E}^{Z}_{11} &\approx \mathbf{a}_1\cdot\mathbf{u}^{Z}_{,1} = \sum_{k=1}^{n}\sum_{\beta=1}^{2}(\mu_{\beta k}\mathbf{a}_1\cdot\mathbf{a}_{\beta,1} + \mu_{\beta k,1}\,\mathbf{a}_1\cdot\mathbf{a}_\beta)w_k\\
\bar{E}^{Z}_{22} &\approx \mathbf{a}_2\cdot\mathbf{u}^{Z}_{,2} = \sum_{k=1}^{n}\sum_{\beta=1}^{2}(\mu_{\beta k}\mathbf{a}_2\cdot\mathbf{a}_{\beta,2} + \mu_{\beta k,2}\,\mathbf{a}_2\cdot\mathbf{a}_\beta)w_k\\
2\bar{E}^{Z}_{12} &\approx \mathbf{a}_1\cdot\mathbf{u}^{Z}_{,2} + \mathbf{a}_2\cdot\mathbf{u}^{Z}_{,1} = \sum_{k=1}^{n}\sum_{\beta=1}^{2}(\mu_{\beta k}(\mathbf{a}_1\cdot\mathbf{a}_{\beta,2} + \mathbf{a}_2\cdot\mathbf{a}_{\beta,1}) + \mu_{\beta k,2}\,\mathbf{a}_1\cdot\mathbf{a}_\beta + \mu_{\beta k,1}\,\mathbf{a}_2\cdot\mathbf{a}_\beta)w_k\\
2\bar{E}^{Z}_{13} &\approx \mathbf{a}_1\cdot\mathbf{u}^{Z}_{,3} + \cancel{\mathbf{a}_3\cdot\mathbf{u}^{Z}_{,1}} = \sum_{k=1}^{n}\sum_{\beta=1}^{2}(\mu_{\beta k}\mathbf{a}_1\cdot\mathbf{a}_\beta)w_{k,3} + \cancel{\sum_{k=1}^{n}\sum_{\beta=1}^{2}(\mu_{\beta k}\mathbf{a}_3\cdot\mathbf{a}_{\beta,1})w_k}\\
2\bar{E}^{Z}_{23} &\approx \mathbf{a}_2\cdot\mathbf{u}^{Z}_{,3} + \cancel{\mathbf{a}_3\cdot\mathbf{u}^{Z}_{,2}} = \sum_{k=1}^{n}\sum_{\beta=1}^{2}(\mu_{\beta k}\mathbf{a}_2\cdot\mathbf{a}_\beta)w_{k,3} + \cancel{\sum_{k=1}^{n}\sum_{\beta=1}^{2}(\mu_{\beta k}\mathbf{a}_3\cdot\mathbf{a}_{\beta,2})w_k}\\
\bar{E}^{Z}_{33} &\approx 0
\end{aligned} \tag{19}$$

It is worth noting that the warping displacement produces also transverse shear strains unlike the standard KL kinematics. In such strain components the part coming from $\mathbf{u}^{Z}_{,1}$ and $\mathbf{u}^{Z}_{,2}$ are canceled in order to avoid terms in w_k considered of higher order compared to $w_{k,3}$. For example, a w_k that is piece-wise linear through the thickness is associated with piece-wise constant transverse shear strains, while their linear variation is neglected. This is analogous to the Reissner–Mindlin shell, where only constant transverse shear strains are associated to the rigid (linear) section kinematics.

A more compact notation, useful for the subsequent developments, is obtained by collecting the in-plane warping strains as

$$\bar{\boldsymbol{\varepsilon}}_p^z = \begin{bmatrix} \bar{E}_{11}^z \\ \bar{E}_{22}^z \\ \bar{E}_{12}^z \end{bmatrix} = \sum_{k=1}^{n} \bar{\boldsymbol{\psi}}_k w_k \quad \text{with} \quad \bar{\boldsymbol{\psi}}_k = \sum_{\beta=1}^{2} \begin{bmatrix} \mu_{\beta k} \mathbf{a}_1 \cdot \mathbf{a}_{\beta,1} + \mu_{\beta k,1} \mathbf{a}_1 \cdot \mathbf{a}_\beta \\ \mu_{\beta k} \mathbf{a}_2 \cdot \mathbf{a}_{\beta,2} + \mu_{\beta k,2} \mathbf{a}_2 \cdot \mathbf{a}_\beta \\ \mu_{\beta k}(\mathbf{a}_1 \cdot \mathbf{a}_{\beta,2} + \mathbf{a}_2 \cdot \mathbf{a}_{\beta,1}) + \mu_{\beta k,2} \mathbf{a}_1 \cdot \mathbf{a}_\beta + \mu_{\beta k,1} \mathbf{a}_2 \cdot \mathbf{a}_\beta \end{bmatrix} \tag{20}$$

and the transverse shear ones as

$$\bar{\boldsymbol{\varepsilon}}_t^z = \begin{bmatrix} 2\bar{E}_{13}^z \\ 2\bar{E}_{23}^z \end{bmatrix} = \sum_{k=1}^{n} \bar{\boldsymbol{\gamma}}_k w_{k,3} \quad \text{with} \quad \bar{\boldsymbol{\gamma}}_k = \sum_{\beta=1}^{2} \begin{bmatrix} \mu_{\beta k} \mathbf{a}_1 \cdot \mathbf{a}_\beta \\ \mu_{\beta k} \mathbf{a}_2 \cdot \mathbf{a}_\beta \end{bmatrix}. \tag{21}$$

Under the condition of large deformations but small strains, it is possible to simplify the generalized strains $\bar{\boldsymbol{\psi}}_k$ and $\bar{\boldsymbol{\gamma}}_k$ by assuming in Eqs. (20) and (21) $\mathbf{a}_\alpha \cdot \mathbf{a}_\beta \approx \mathbf{A}_\alpha \cdot \mathbf{A}_\beta$, $\mathbf{a}_\alpha \cdot \mathbf{a}_{\beta,1} \approx \mathbf{A}_\alpha \cdot \mathbf{A}_{\beta,1}$ and $\mathbf{a}_\alpha \cdot \mathbf{a}_{\beta,2} \approx \mathbf{A}_\alpha \cdot \mathbf{A}_{\beta,2}$ with $\alpha, \beta = 1, 2$, so that they become independent from the displacement of the reference surface:

$$\bar{\boldsymbol{\psi}}_k \approx \sum_{\beta=1}^{2} \begin{bmatrix} \mu_{\beta k} \mathbf{A}_1 \cdot \mathbf{A}_{\beta,1} + \mu_{\beta k,1} \mathbf{A}_1 \cdot \mathbf{A}_\beta \\ \mu_{\beta k} \mathbf{A}_2 \cdot \mathbf{A}_{\beta,2} + \mu_{\beta k,2} \mathbf{A}_2 \cdot \mathbf{A}_\beta \\ \mu_{\beta k}(\mathbf{A}_1 \cdot \mathbf{A}_{\beta,2} + \mathbf{A}_2 \cdot \mathbf{A}_{\beta,1}) + \mu_{\beta k,2} \mathbf{A}_1 \cdot \mathbf{A}_\beta + \mu_{\beta k,1} \mathbf{A}_2 \cdot \mathbf{A}_\beta \end{bmatrix} \quad \bar{\boldsymbol{\gamma}}_k \approx \sum_{\beta=1}^{2} \begin{bmatrix} \mu_{\beta k} \mathbf{A}_1 \cdot \mathbf{A}_\beta \\ \mu_{\beta k} \mathbf{A}_2 \cdot \mathbf{A}_\beta \end{bmatrix}. \tag{22}$$

We can note that, in the simplified form, the generalized strains defined in the previous equation are linear in the warping amplitudes and their derivatives. Moreover, the generalized transverse shear strains depends only on the warping amplitudes, so that, the discrete version of model will be automatically free from transverse shear locking. From this point of view, the proposed model can be seen as a generalization of the one proposed in [34] for shear-deformable shells, that can be recovered by selecting the warping profile as a linear function of the thickness coordinate (plane section hypothesis).

2.3. Remarks on the geometrical exactness of the hierarchic shell

It is worth noting that the large deformation/small strain hierarchic shell model formulated above is geometrically exact, a term commonly used to mean that the strain measure is not affected by rigid body motions of arbitrary magnitude and, then, by changes of observer. This fact is easy to prove and is inherent in the hierarchical theory. Indeed, rigid motions are described in terms of displacement of the shell reference surface only. This means that they do not contribute to the warping part of the strain, which becomes clear also by looking at Eq. (22), and the warping displacement is purely deformational. The additive split of the total Green–Lagrange strain in Eq. (18) into warping part and basic Kirchhoff–Love geometrically exact part makes the proof of invariance of the total strain under superposition of rigid motions trivial.

2.4. From covariant to local cartesian strain components

The total covariant strain components collected in Voigt notation can be written as

$$\bar{\boldsymbol{\varepsilon}}_p = \bar{\mathbf{e}} + \xi^3 \bar{\boldsymbol{\chi}} + \sum_{k=1}^{n} \bar{\boldsymbol{\psi}}_k w_k \qquad \bar{\boldsymbol{\varepsilon}}_t = \sum_{k=1}^{n} \bar{\boldsymbol{\gamma}}_k w_{k,3} \tag{23}$$

where the transverse shear ones coincide with the warping contribution. In order to impose the constitutive law, it is convenient to express the strain components in a local Cartesian coordinate system whose $x-y$ plane is tangent to the shell reference surface. For a general 3D continuum, this transformation is reported, for instance, in [23,25]. The simplification of this transformation accounting for the Kirchhoff–Love shell hypothesis and neglecting its variation through the thickness furnishes the sought relationship:

$$\begin{aligned} \boldsymbol{\varepsilon}_p &= \mathbf{T}_p \bar{\boldsymbol{\varepsilon}}_p \quad \text{with} \quad \mathbf{T}_p = \begin{bmatrix} x_\xi^2 & x_\eta^2 & 2x_\xi x_\eta \\ y_\xi^2 & y_\eta^2 & 2y_\xi y_\eta \\ x_\xi y_\xi & x_\eta y_\eta & x_\xi y_\eta + x_\eta y_\xi \end{bmatrix}^{-T} \\ \boldsymbol{\varepsilon}_t &= \mathbf{T}_t \bar{\boldsymbol{\varepsilon}}_t \quad \text{with} \quad \mathbf{T}_t = \begin{bmatrix} x_\xi & x_\eta \\ y_\xi & y_\eta \end{bmatrix}^{-T}. \end{aligned} \tag{24}$$

The coefficients of the transformation matrices are $x_\xi = \mathbf{i}_1 \cdot \mathbf{A}_1$, $y_\xi = \mathbf{i}_2 \cdot \mathbf{A}_1$, $x_\eta = \mathbf{i}_1 \cdot \mathbf{A}_2$, $y_\eta = \mathbf{i}_1 \cdot \mathbf{A}_2$ with $\mathbf{i}_1$ and $\mathbf{i}_2$ the unit vectors along the axis of the local Cartesian coordinates where the material properties are defined.

2.5. Pre-integration of the elasticity matrices

For a linear elastic material, e.g. isotropic, the constitutive matrices linking stress and strain are

$$\mathbf{C}_p = \frac{E}{1-\nu^2} \begin{bmatrix} 1 & \nu & 0 \\ \nu & 1 & 0 \\ 0 & 0 & (1-\nu)/2 \end{bmatrix} \qquad \mathbf{C}_t = \begin{bmatrix} G & 0 \\ 0 & G \end{bmatrix} \tag{25}$$

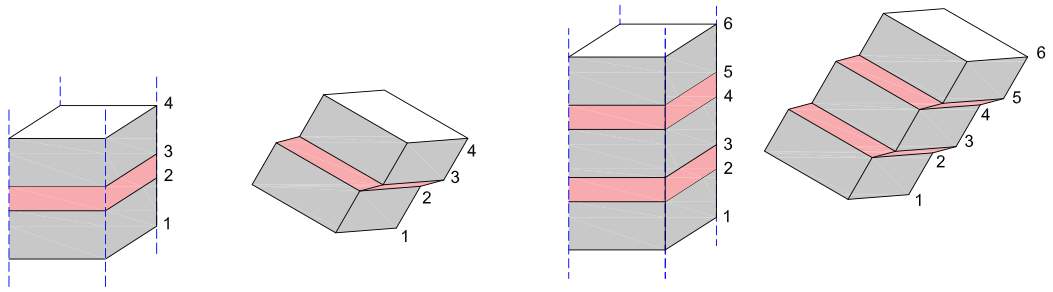

(a) 3 layers (b) 5 layers

Fig. 1. Kinematics of laminates with alternating stiff/soft layers.

where $\mathbf{C}_p$ is the plane stress matrix and $\mathbf{C}_t$ is a diagonal matrix made with the shear modulus of the material. Collecting the local Cartesian generalized in-plane and transverse strains in vectors

$$\boldsymbol{\varepsilon}_P = \begin{bmatrix} \mathbf{e} \\ \boldsymbol{\chi} \\ \boldsymbol{\psi}_1 \\ \vdots \\ \boldsymbol{\psi}_n \end{bmatrix} \qquad \boldsymbol{\varepsilon}_T = \begin{bmatrix} \boldsymbol{\gamma}_1 \\ \vdots \\ \boldsymbol{\gamma}_n \end{bmatrix} \tag{26}$$

obtained from the covariant ones through Eq. (24), the equivalence of strain energy per unit of reference surface

$$W = \frac{1}{2}\int_{\xi_b^3}^{\xi_t^3} (\boldsymbol{\varepsilon}_p^T \mathbf{C}_p \boldsymbol{\varepsilon}_p + \boldsymbol{\varepsilon}_t^T \mathbf{C}_t \boldsymbol{\varepsilon}_t) d\xi^3 = \frac{1}{2}(\boldsymbol{\varepsilon}_P^T \mathbf{D}_P \boldsymbol{\varepsilon}_P + \boldsymbol{\varepsilon}_T^T \mathbf{D}_T \boldsymbol{\varepsilon}_T) \tag{27}$$

provides the generalized constitutive matrices

$$\mathbf{D}_P = \begin{bmatrix} \mathbf{D}_{mm} & \mathbf{D}_{mb} & \mathbf{D}_{mw_1} & \cdots & \mathbf{D}_{mw_n} \\ & \mathbf{D}_{bb} & \mathbf{D}_{bw_1} & \cdots & \mathbf{D}_{bw_n} \\ & & \mathbf{D}_{w_1w_1} & \cdots & \mathbf{D}_{w_1w_n} \\ & \text{sym} & & \ddots & \vdots \\ & & & & \mathbf{D}_{w_nw_n} \end{bmatrix} \quad \mathbf{D}_T = \begin{bmatrix} \mathbf{D}_{T11} & \cdots & \mathbf{D}_{T1n} \\ & \ddots & \vdots \\ \text{sym} & & \mathbf{D}_{Tnn} \end{bmatrix}$$

where

$$\mathbf{D}_{mm} = \int_{\xi_b^3}^{\xi_t^3} \mathbf{C}_p \qquad \mathbf{D}_{mb} = \int_{\xi_b^3}^{\xi_t^3} \xi^3 \mathbf{C}_p \qquad \mathbf{D}_{mw_k} = \int_{\xi_b^3}^{\xi_t^3} w_k \mathbf{C}_p$$

$$\mathbf{D}_{bb} = \int_{\xi_b^3}^{\xi_t^3} \xi^3 \xi^3 \mathbf{C}_p \qquad \mathbf{D}_{bw_k} = \int_{\xi_b^3}^{\xi_t^3} \xi^3 w_k \mathbf{C}_p \qquad \mathbf{D}_{w_iw_j} = \int_{\xi_b^3}^{\xi_t^3} w_i w_j \mathbf{C}_p$$

$$\mathbf{D}_{Tij} = \int_{\xi_b^3}^{\xi_t^3} w_{i,3}\, w_{j,3}\, \mathbf{C}_t.$$

Each sub-matrix is obtained in the pre-processing stage by integrating over the shell thickness. The integrals are calculated as a discrete sums of contributions of each layer to take into account the change of material properties through the thickness.

3. Modeling laminates with alternating layup

In this section, focus is given to possible choices of the warping model for composite shells with alternating stiff/soft layers. Typical examples are polymer-metal composites and glass laminates. In this last case, the stiff parts are glass layers coupled by soft parts usually made of PVB or silicone. When the stiffness of the two material types differ of many orders of magnitude, the hypotheses of plane section remaining plane after deformation becomes unreliable and the solution obtained by the first order plate theory inaccurate, even using shear correction factors. The typical kinematics is depicted in Fig. 1 for the example case of 3 and 5 layers respectively. Solid models can be used to obtain a reliable solution by discretizing the structure also through the thickness. However, general purpose solid finite elements are not suitable for layered plates because of the high number of DOFs. The KL model hierarchically enhanced by warping can be adopted for a simple and efficient modeling of this class of composites, after a proper selection of the warping profile.

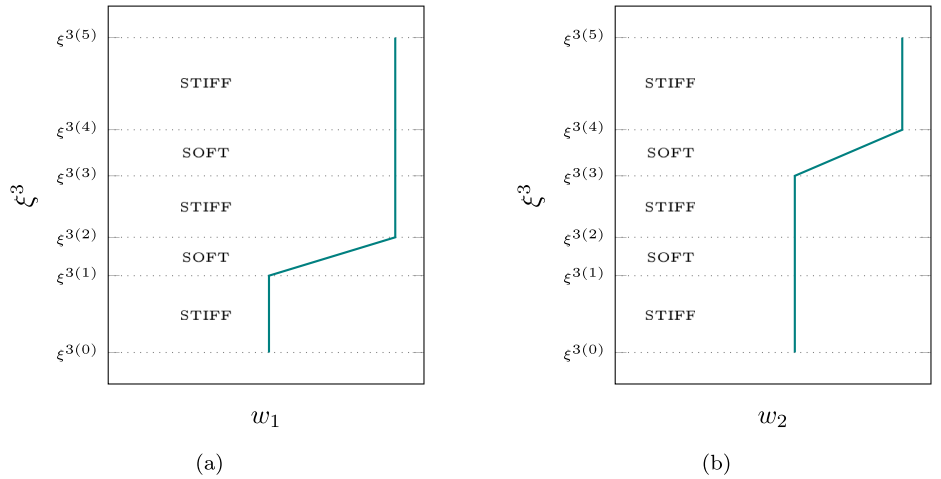

Fig. 2. Warping functions with independent transverse shear deformations of the soft interlayers (WI) for 5 alternating stiff/soft layers.

3.1. Warping profile with independent transverse shear deformations of the soft layers

The alternating layup induces a specific deformation pattern, which distinguishes them from other composites [22,30]. The transverse shear strains tend to concentrate in the soft interlayers, with a nearly constant distribution in the thickness, while they are negligible in the stiff plies. Moreover, although the interlayers are soft, the bonding capacity is such that the stiff layers are all subjected to almost identical rotations with respect with their normals in the undistorted configuration. The warping profile is chosen as proposed for the first time in [22]. In practice, a number of warping profiles equal to the soft interlayers is considered. The generic warping function w_k is defined layer-wise as

$$w_k(\xi^3) = \begin{cases} -1 & \text{if} \quad \xi^3 < \xi^3_{bk} \\ \dfrac{2(\xi^3 - \xi^3_{bk})}{t_k} - 1 & \text{if} \quad \xi^3_{bk} \le \xi^3 \le \xi^3_{tk} \\ 1 & \text{if} \quad \xi^3 > \xi^3_{tk} \end{cases} \tag{28}$$

where t_k is the thickness of the kth soft layer whose bottom and top interface are located at ξ^3_{bk} and ξ^3_{tk} respectively. For instance, in the case of 3 layers the warping profile at the 4 interfaces of the laminate is $\{-1,-1,1,1\}$. In the 5 layers case, the two warping profiles at the 6 interfaces are $\{-1,-1,1,1,1,1\}$ and $\{-1,-1,-1,-1,1,1\}$. A rigid translation is conveniently subtracted from the warping shapes such that $w_k(\xi^3_r) = 0$ for a correct imposition of the boundary conditions on the reference surface corresponding to $\xi^3 = \xi^3_r$. The same profiles, but with independent amplitudes, can be assumed along both the directions defined by the tangent vectors $\mathbf{A}_1$ and $\mathbf{A}_2$. The total number of variables of the model at each point over the shell surface is $n_t = 3 + 2n_s$: 3 components of the reference surface displacement and 2 amplitudes for the warping profile associated to each of the n_s soft layers. For the case of 5 layers, the 2 warping functions are illustrated in Fig. 2. Compared to the co-rotational shell model proposed in [22], our proposal is purely Total Lagrangian, i.e. the strain measure accuracy is not affected by the mesh size, and the number of variables is reduced by imposing that all stiff layers maintain the same director orthogonal to the deformed surface.

3.2. Warping profile with a single zigzag shape

The refined ZZT provides a single piecewise linear shape of the warping profile over the whole thickness of the laminate, denoted in following as $w(\xi^3)$, avoiding the subscript k previously used in the case of multiple shapes. According to this theory, the zigzag function is defined by the $N+1$ interface values $w^{(j)}$, with $j = 0, 1, \dots, N$ and N the overall number of layers. The theory sets $w(\xi^3)$ to vanish at the top and bottom surfaces of the laminate, i.e. $w^{(0)} = w^{(N)} = 0$. The internal interface values are computed as

$$w^{(j)} = w^{(j-1)} + h^{(j)}\beta^{(j)} \quad \text{with} \quad j = 1, \dots, N-1 \tag{29}$$

where $h^{(j)}$ is the thickness of the jth layer. $\beta^{(j)}$ is the slope of the zigzag function in each layer j, and is obtained as

$$\beta^{(j)} = \frac{\bar{G}}{G^{(j)}} - 1 \quad \text{with} \quad j = 1, \dots, N \tag{30}$$

where $G^{(j)}$ is the shear modulus of the jth layer and $\bar{G}$ denotes a weighted average of G over the laminate thickness, i.e.

$$\bar{G} = \left(\frac{1}{h} \sum_{j=1}^{N} \frac{h^{(j)}}{G^{(j)}} \right)^{-1} \tag{31}$$

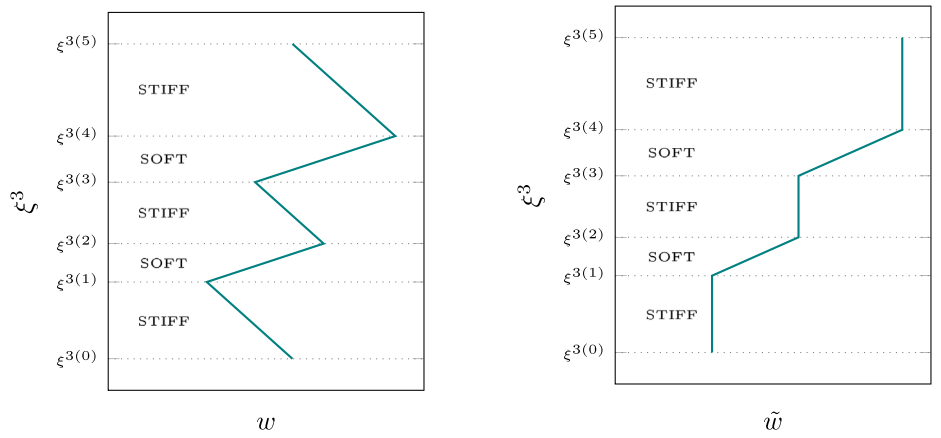

(a) ZZ function (b) Rotated ZZ function

Fig. 3. Zigzag warping function (WZ) for 5 alternating stiff/soft layers: the function coming from the refined ZZT on the left and the function rotated in order to minimize the shear deformation of the stiff layers on the right.

The complete derivation of these equations can be found in [36]. Let us consider a layup made of 5 alternating stiff/soft layers. As we can observe on the left side of Fig. 3, the constraint of vanishing zigzag function at the top and bottom surfaces produces a profile characterized by non-null slop, and then transverse shear strain, in all layers including the stiff ones.

Instead, it was demonstrated in a number of papers, e.g. in [22], that the transverse shear strains tend to vanish in the stiff layers. This is not an issue when the zigzag function is used to enhance shear deformable beam and shell models, because the transverse shear strains of the basic models can compensate for the additional part coming from the zigzag function, so recovering the Kirchhoff–Love behavior of the stiff layers. The price to pay, in this case, is the need for independent rotational DOFs for describing the section rotation, complicating also the expressions for finite 3D rotations. Instead, if we want to avoid these additional variables and to keep using the proposed Kirchhoff–Love model hierarchically enhanced with warping, it is necessary to modify the zigzag function in such a way as to minimize the slop of the zigzag function in the stiff layer. We propose a formula to rotate the zigzag shape. Starting from the one obtained with the formulas above, the rotated zigzag function $\tilde{w}$ is obtained as

$$\tilde{w}(\xi^3) = w(\xi^3) - \varphi\xi^3 \quad \text{with} \quad \varphi = \frac{\sum_{j=1}^{N} G^{(j)} h^{(j)} \beta^{(j)}}{\sum_{j=1}^{N} G^{(j)} h^{(j)}} \tag{32}$$

where φ represents a weighted average of the zigzag function slop over the laminate thickness, in order to concentrate the transverse shear deformation in the soft layers only. Finally, a rigid displacement, e.g. the value of $\tilde{w}(\xi^3)$ at the reference shell surface, can be also subtracted to $\tilde{w}$ for an easy imposition of the support boundary condition. The rotated zigzag function is illustrated on the right side of Fig. 3 for a layup with 5 alternating stiff/soft layers. The resulting shell model is accurate also when the zigzag effects become important, although based on just 5 DOFs per reference surface point, i.e. 3 displacements and the 2 amplitudes of $\tilde{w}$ along the two directions identified by the tangent vectors $\mathbf{A}_1$ and $\mathbf{A}_2$, regardless of the number of layers. In the limit case of stiffness ratio tending to infinity, the approach is equivalent to the one proposed in [37] for enhancing a linear Euler–Bernoulli beam, where $\tilde{w}(\xi^3)$ is defined as $w(\xi^3) + \xi^3$.

3.3. Remarks on the warping models

The warping models presented above for alternating layups exploit the Kirchhoff–Love hypothesis of negligible transverse shear deformations in the stiff layers confirmed in the literature (e.g. [22]). Along with the assumption of equal director in all stiff layers, this allows to reduce drastically the number of DOFs compared to a 3D model without losing accuracy in the predictions of interest: displacements, stability, in-plane stresses in the stiff layers and transverse shear deformations in the soft interlayers.

The stiff layers behave as thin shells loosely coupled by the interlayers. Therefore, the in-plane stresses prevail over the transverse shear stresses in those layers in the strength check. An accurate prediction of transverse shear strains is required in the soft interlayers to check the bonding capacity. These can be computed directly from the proposed kinematics and the corresponding stresses via the constitutive law.

The only information not directly available with the suggested warping models is the transverse shear stresses inside the stiff layers. As standard when using the Kirchhoff–Love assumption, they can be accurately obtained from the in-plane stresses by an equilibrium-based post-processing (e.g. see [4]). Alternatively, since the proposed hierarchic shell model can deal with an arbitrary number of warping functions, additional warping shapes and the corresponding amplitudes can be added to the kinematics to model directly the transverse shear deformations in the stiff layers and computing the corresponding stresses via the constitutive law. However, neither approach is worthy of a further discussion for stiff/soft layups, where the transverse shear effects inside the stiff layers are actually of little significance [22].

4. Effective isogeometric formulation

4.1. The isogeometric shell element

Following the isoparametric concept, geometry and displacement field of the reference surface and warping amplitudes are approximated, over each element, as follows

$$\mathbf{X}(\xi,\eta)=\mathbf{N}_u(\xi,\eta)\mathbf{X}_e,\quad \mathbf{u}(\xi,\eta)=\mathbf{N}_u(\xi,\eta)\mathbf{d}_e,\quad \boldsymbol{\mu}(\xi,\eta)=\mathbf{N}_\mu(\xi,\eta)\boldsymbol{\mu}_e \tag{33}$$

where $\mathbf{X}_e$, $\mathbf{d}_e$ and $\boldsymbol{\mu}_e$ collect the discrete parameters at the control points of the element associated to geometry, reference surface displacement and warping amplitudes respectively. The matrices $\mathbf{N}_u(\xi,\eta)$ and $\mathbf{N}_\mu(\xi,\eta)$ collect bivariate NURBS functions [38]. Exploiting the isogeometric approximation, the strain components become

$$\boldsymbol{\varepsilon}_P=\boldsymbol{\varepsilon}_P(\mathbf{q}_e)\qquad \boldsymbol{\varepsilon}_T=\boldsymbol{\varepsilon}_T(\mathbf{q}_e)\quad\text{with}\quad \mathbf{q}_e=\begin{bmatrix}\mathbf{d}_e\\ \boldsymbol{\mu}_e\end{bmatrix}. \tag{34}$$

4.2. Strain energy, discrete operators and equilibrium path

Collecting in vector $\mathbf{q}$ all the DOFs for the approximation of the reference surface displacement and the warping amplitudes over the structure, the overall strain energy can be expressed as a sum of element contributions $\Phi(\mathbf{q})\equiv\sum_e\Phi_e(\mathbf{q}_e)$, where the element strain energy can be decomposed into in-plane and transverse part as

$$\Phi_e(\mathbf{q}_e)\equiv\Phi_{Pe}(\mathbf{q}_e)+\Phi_{Te}(\mathbf{q}_e)\quad\text{with}\quad\begin{cases}\Phi_{Pe}(\mathbf{q}_e)=\displaystyle\int_{\Omega_e}\left(\frac{1}{2}\boldsymbol{\varepsilon}_P^T\mathbf{D}_P\boldsymbol{\varepsilon}_P\right)d\Omega_e\\ \Phi_{Te}(\mathbf{q}_e)=\displaystyle\int_{\Omega_e}\left(\frac{1}{2}\boldsymbol{\varepsilon}_T^T\mathbf{D}_T\boldsymbol{\varepsilon}_T\right)d\Omega_e\end{cases} \tag{35}$$

where Ω_e is the element domain. It is worth highlighting that the model is path-independent for conservative external loads, since it is based on the total elastic potential parametrized in terms of displacement variables. The differentiation of the generalized strains in Eq. (34) provides the tangent compatibility operators

$$\mathbf{B}_P(\mathbf{q}_e)=\frac{\partial\boldsymbol{\varepsilon}_P}{\partial\mathbf{q}_e}\qquad\mathbf{B}_T=\frac{\partial\boldsymbol{\varepsilon}_T}{\partial\mathbf{q}_e} \tag{36}$$

where $\mathbf{B}_P$ is a function of the discrete DOFs, while $\mathbf{B}_T$ is constant considering the simplified strain expression in Eq. (22). The internal force vector of the element can be then evaluated as

$$\mathbf{s}_e(\mathbf{q}_e)\equiv\frac{\partial\Phi_e}{\partial\mathbf{q}_e}=\mathbf{s}_{Pe}(\mathbf{q}_e)+\boldsymbol{K}_{Te}\mathbf{q}_e\quad\text{with}\quad\begin{cases}\mathbf{s}_{Pe}(\mathbf{q}_e)=\displaystyle\int_{\Omega_e}\left(\mathbf{B}_P(\mathbf{q}_e)^T\mathbf{D}_P\boldsymbol{\varepsilon}_P(\mathbf{q}_e)\right)d\Omega_e\\ \boldsymbol{K}_{Te}=\displaystyle\int_{\Omega_e}\left(\mathbf{B}_T^T\mathbf{D}_T\mathbf{B}_T\right)d\Omega_e\end{cases} \tag{37}$$

where $\mathbf{s}_{eT}(\mathbf{q}_e)$ is the contribution to the element internal forces due to the in-plane strains and $\boldsymbol{K}_{Te}$ is the constant element stiffness matrix associated to the transverse shear strains. A further differentiation provides the element tangent stiffness matrix as

$$\boldsymbol{K}_e(\mathbf{q}_e)\equiv\frac{\partial\mathbf{s}_e}{\partial\mathbf{q}_e}=\boldsymbol{K}_{Pe}(\mathbf{q}_e)+\boldsymbol{K}_{Te} \tag{38}$$

where

$$\boldsymbol{K}_{Pe}(\mathbf{q}_e)=\int_{\Omega_e}\left(\mathbf{B}_P(\mathbf{q}_e)^T\mathbf{D}_P\mathbf{B}_P(\mathbf{q}_e)+\mathbf{G}(\mathbf{q}_e,\boldsymbol{\sigma}_P(\mathbf{q}_e))\right)d\Omega_e\quad\text{with}\quad\boldsymbol{\sigma}_P(\mathbf{q}_e)=\mathbf{D}_P\boldsymbol{\varepsilon}_P(\mathbf{q}_e) \tag{39}$$

and the geometric contribution $\mathbf{G}$ is defined as

$$\mathbf{G}(\mathbf{q}_e,\boldsymbol{\sigma}(\mathbf{q}_e))=\sum_{k=1}^{6}\sigma_{Pk}\boldsymbol{\Psi}_k(\mathbf{q}_e)\quad\text{with}\quad\boldsymbol{\Psi}_k(\mathbf{q}_e)=\frac{\partial^2\varepsilon_{Pk}}{\partial\mathbf{q}_e^2} \tag{40}$$

since only the first six components of $\boldsymbol{\sigma}_P$, i.e. membrane strains and curvatures, are nonlinear in the discrete DOFs.

The equilibrium of slender elastic structures subject to conservative loads amplified by a proportionality factor λ is expressed by the discrete version of the virtual work equation:

$$\mathbf{r}(\mathbf{q},\,\lambda)\equiv\mathbf{s}(\mathbf{q})-\lambda\,\mathbf{f}=\mathbf{0}, \tag{41}$$

where $\mathbf{r}:\mathbb{R}^{N+1}\to\mathbb{R}^N$ is a nonlinear vectorial function of the vector $\{\mathbf{q},\lambda\}\in\mathbb{R}^{N+1}$, collecting the configuration $\mathbf{q}\in\mathbb{R}^N$ and the load multiplier $\lambda\in\mathbb{R}$, $\mathbf{s}(\mathbf{q})$ is the global internal force vector and $\mathbf{f}$ the reference load vector. Eq. (41) represents a system of N equations and $N+1$ unknowns and its solutions define the *equilibrium paths* as curves in $\mathbb{R}^{N+1}$. The Riks arc-length method [39] is the general solution strategy to trace these curves in a step-by-step manner from a known initial configuration $\mathbf{q}_0$ corresponding to $\lambda=0$. At each step some Newton iterations are needed to solve (41), with the Jacobian involving the global tangent stiffness matrix, obtained by assembling the element ones in Eq. (38). Load-controlled and displacement-controlled schemes are recovered as a particular choice of Riks constraint surface [40].

4.3. Remarks on the iterative solution

Robustness and efficiency of the iterative solution are achieved by using the mixed integration point (MIP) strategy [40,41], particularly suitable for the considered problem. It was already demonstrated in many works (see e.g. [40–43] how the MIP approach improves the convergence behavior of the Newton iterations of displacement-based formulations in large deformations, providing a comparable robustness (large steps with few iterations) as that observed in mixed/hybrid finite element formulations [23,44] for solids, shells and beams. For the basic Kirchhoff–Love model, the excellent iterative performances are demonstrated in [3]. Since the new shell model proposed in this work is an enrichment of the Kirchhoff–Love one where the additional displacement and strain are linear in the warping DOFs, i.e. not affecting the model nonlinearity, the proposal is characterized by an identical iterative behavior as that reported in [3]. The incremental-iterative procedure used for the numerical tests follows exactly that detailed in [40] based on MIP method and adaptive step size. In particular, all the details concerning stepping scheme, convergence criterion and metric factors of the Riks method are reported in the Implementation details Section 4.1 of [40]. The only parameters to be defined by the user are the maximum load and the initial step length at the first load increment. This is set as 0.05 of the maximum load for all the numerical tests in this paper, unless otherwise stated.

4.4. Locking, NURBS selection and patch-wise selective reduced integration

It is worth noting that the transverse shear strains are linear functions of the warping amplitudes (no derivatives) only. This means that they are naturally free from locking and, then, the associated stiffness matrix $\boldsymbol{K}_{Te}$ can be evaluated, only once since independent from $\mathbf{q}$, by a full numerical integration. Instead, the in-plane strains are affected by membrane locking as in the standard KL model, also for initially flat plates undergoing finite deformations. To avoid such an undesired inaccuracy one could use NURBS with a very high order, but this would compromise the efficiency due to the reduced sparsity and the greater number of integration points. Instead we propose a selective reduced integration for the internal forces $\mathbf{s}_{Pe}$ and tangent stiffness $\boldsymbol{K}_{Pe}$ associated to the in-plane strains. Among all possible schemes, we adopt the patch-wise reduced integration named S_0^3 (notation according to [45]) that was identified in [3] as the best solution to avoid locking with cubic NURBS basis functions with C^2 continuity for the standard KL model without spurious modes. The notation means that points and weights are defined over the patch in order to integrate exactly functions of order 3 and C^0 continuity. The corresponding points and weights depend on the knot vector (mesh) and can be found using the algorithm provided in [46], that is simple and inexpensive. Beside the locking issue, the scheme S_0^3 is very efficient because of the very small number of integration points, asymptotically about 1.5×1.5 points per cubic element. Number and position of the points is not equal in each element, but they are distributed over the patch to take into account the inter-element high continuity. Concerning the number of discrete DOFs, it is worth noting that C^2 cubic NURBS are based on $(n_{e1}+3)\times(n_{e2}+3)$ control points, where n_{e1} and n_{e2} are the number of elements in the two parametric directions, i.e. asymptotically one control point per element. This is a great advantage over high order Lagrangian finite elements.

5. Numerical tests

The proposed isogeometric Kirchhoff–Love model hierarchically enhanced with warping profiles is tested in a sample of numerical experiments concerning both plane and curved structures undergoing buckling and large deflections. The two warping models described in Section 3 are employed. Comparisons are made between the models below.

- KL: Basic Kirchhoff–Love shell model without warping;
- KLWI: Hierarchic Kirchhoff–Love shell model with the warping model of Section 3.1 based on independent shear deformations of the soft layers;
- KLWZ: Hierarchic Kirchhoff–Love shell model with the warping model of Section 3.2 based on a single zigzag function;
- FSDT: Mindlin–Reissner shell model (FSDT) of Abaqus with shear correction factors;
- 3D: fully solid model of Abaqus with through-the-thickness discretization assumed as reference solution.

The basic KL can be recovered by constraining the warping amplitudes of KLWI and KLWZ to vanish all over the domain.

The layups illustrated in Fig. 4 are considered in the simulations. The elastic parameters of the stiff layers are typical of soda-lime glass, whereas the stiffness of the interlayers may be representative of silicone, polyvinyl butyral and ionoplast SentryGlas. It is worth noting that only a warping function is used in KLWI for 3-layer layups to capture the sliding of the soft layer and this is the same as that of KLWZ for large stiffness ratios of the materials. Therefore, the two models coincides in this case. Instead, they are different for layups with more than 3 layers: KLWI utilizes $3+2n_s = 2+N$ DOFs per surface point with n_s the number of soft layers and N the total number of layers, while KLWZ only 5 DOFs regardless of the number of layers.

In order to summarize the cost of the different models in terms of unknowns, the corresponding number of DOFs per surface point is reported in Table 1.

It is worth noting that the 3D solution obtained with quadratic FEs is also quite well reproduced by the Abaqus linear solid-shell FEs (one per layer), that however, still requires many more DOFs than the shell models, including the proposed ones. Besides the number of unknowns, a significant advantage of 2D models is that no numerical integration is required through the thickness, with a further reduction of the number of operations. In addition, a nice feature of the proposals KLWZ and KLWI is that the strain measure is nonlinear only in the 3 reference surface displacement DOFs and linear in the others (see Eqs. (22) and (37)), with a consequent reduced complexity in the computation of internal forces and tangent stiffness matrix compared to 3D models nonlinear in all the

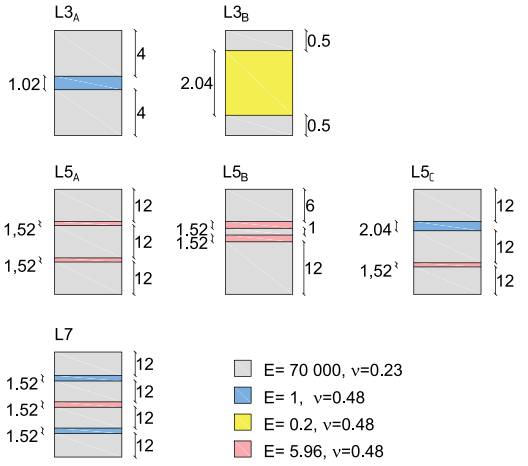

Fig. 4. Illustration of the layups used in the analyses in terms of number, thickness (mm), Young modulus E (MPa) and Poisson coefficient of the layers.

Table 1
Number of unknowns per surface point of the different models.

Layers	KL	FSDT	KLWZ	KLWI	Solid-shell	3D
N	3	5	5	$2+N$	$3(N+1)$	$3(2N+1)$
3	3	5	5	5	12	21
5	3	5	5	7	18	33
7	3	5	5	9	24	45

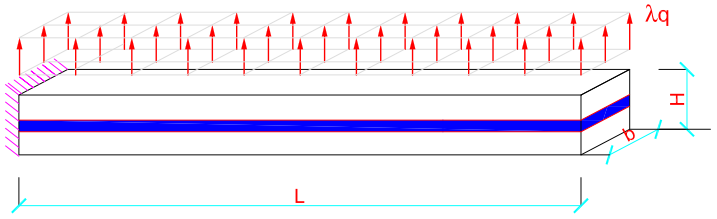

Fig. 5. Cantilever beam under transverse load: geometry, load, and boundary conditions.

DOFs. The basic KL is the most efficient choice, but it tends to be largely overstiff for the considered laminates. It is included in the results to quantify how much the section warping affects the prediction. The Abaqus FSDT shell model has the same number of DOFs as KLWZ, but it considers warping only indirectly and approximatively by means of shear correction factors tuned for laminates. However, this model becomes unreliable for high stiffness ratios of the layers, as occurs for typical alternating laminates.

The numerical results will focus on the main outputs governing the mechanical behavior of alternating laminates with high stiffness ratios:

- load–displacement curves;
- in-plane stresses in the stiff layers;
- transverse shear strains in the soft interlayers.

5.1. Multi-layer cantilever beam

5.1.1. Large deflection due to a transverse distributed load

The first test displays the nonlinear analysis of a cantilever beam of length $L = 500$ mm and and $b = 10$ mm subjected to a distributed transversal load on the top stiff layer as illustrated in Fig. 5. To begin with, the stacking sequences $L3_A$ and $L3_B$ are considered. The reference surface load is $q = 10^{-3}$ MPa for $L3_A$ and $q = 10^{-4}$ MPa for $L3_B$.

The beam is analyzed with the KLWI model (coincident with KLWZ) and different meshes varying the number of elements along the length. The finest mesh is considered for the basic KL solution. The load factor vs. tip displacement equilibrium curve is reported in Fig. 6 for the two layups and using the different models. The transverse component w and the axial component u are monitored. As can be seen from the comparison between the different meshes adopted, the rate of convergence of the model is remarkable. The comparison shows a very good performance of the proposed solution, given the good agreement with the 3D solution. On the

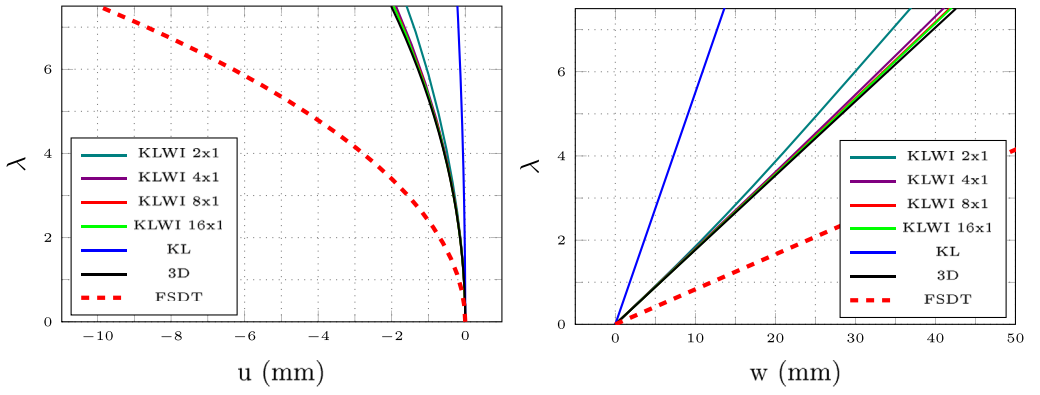

(a) Layup $L3_A$

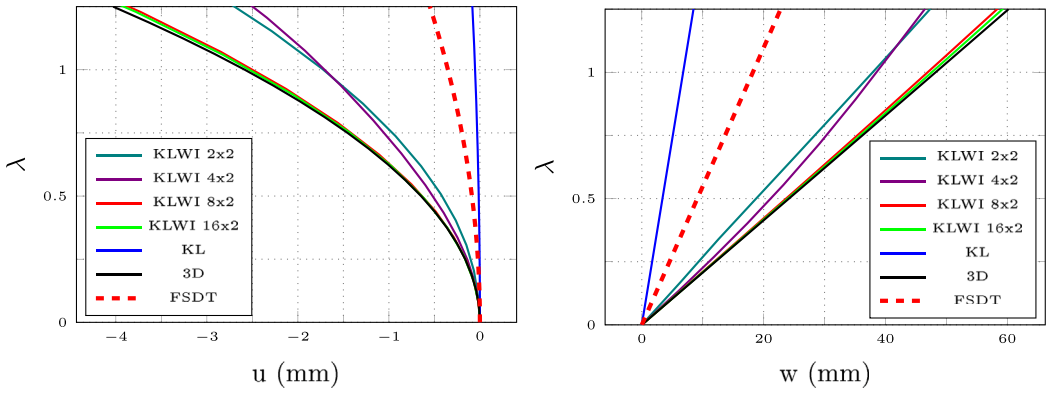

(b) Layup $L3_B$

Fig. 6. Cantilever beam under transverse load: comparison of the equilibrium path in terms of vertical (w) and axial (u) displacement components at the free end obtained by KLWI and KL shell model with solid model and FSDT shell model of Abaqus.

contrary, the lack of transverse shear deformations in the basic KL model brings to over-stiff solutions. Also the shear deformable shell model of Abaqus is inaccurate for this class of composites because the adopted shear correction factors become unreliable for large stiffness ratios of the materials and will be discarded in the other tests. Subsequently, the same beam is analyzed with all the other layups to compare KLWI with KLWZ for more than 3 layers. Table 2 shows the linear elastic solution for the tip displacement considering $q = 10^{-3}$ MPa and a converged mesh. It is possible to observe that KLWI demonstrates to be robust for every type of alternating layups. KLWZ provides the same results for $L5_A$ (uniform stiff layers and uniform soft layers) and $L5_B$ (non-uniform stiff layers and uniform soft layers) with a reduced number of DOFs with respect to KLWZ, but its prediction is inaccurate for $L5_C$ (non-symmetric) and $L7$ (symmetric), both characterized by non-uniform soft layers. This holds also varying the beam length as reported in Tables 2 and 2, apart from very slender cases for which warping gets less important. The reason of this inaccuracy for non-uniform soft layers can be understood by looking at Fig. 7, showing the ratio of the transverse shear deformations of the soft layers for $L5_C$ (two soft layers, i.e. 2 and 4) and $L7$ (three soft layers, i.e. 2, 4 and 6) obtained for the linear elastic solution. It can be seen that the ratio of the transverse shear deformations among non-uniform soft layers varies with the beam length. This means that KLWZ, based on a single zigzag function constraining this deformation ratio, cannot capture the correct behavior. This means that a single zigzag function, whatever it is, is not sufficient in case of non-uniform soft layers, even for symmetric stacking sequences as $L7$.

5.1.2. Buckling under compression

The same cantilever beam seen in the previous test is now subjected to a compression load on the glass layers at the free end section, as described in Fig. 8. The layups $L3_A$ and $L3_B$ are considered. The reference edge compression load is $q = h_{st} \cdot 1$ MPa, with h_{st} (mm) the sum of the thicknesses of the stiff layers. The reference shell surface corresponds to the middle surface of the laminate.

The same meshes considered in the previous example are adopted here, comparing the KLWI model (equivalent to KLWZ) to the basic KL model and the 3D results. In order to avoid the bifurcation jump of the perfect structure after almost null pre-buckling deformations, a small transverse tip edge load of magnitude $q \cdot 10^{-4}$ is applied as an out-of-plane imperfection. Fig. 9 shows the

Table 2
Cantilever beam under transverse load: Converged linear elastic tip transverse displacement (mm) varying layup and beam length for KLWI and KLWZ shell models and 3D model.

(a) Beam length $L = 500$ mm

Layup	KLWI	KLWZ	3D
$L5_A$	1.13e−1	1.13e−1	1.13e−1
$L5_B$	3.87e−1	3.87e−1	3.88e−1
$L5_C$	1.51e−1	8.73e−2	1.52e−1
$L7$	1.17e−1	7.65e−2	1.17e−1

(b) Layup $L5_C$ varying the beam length

L(mm)	KLWI	KLWZ	3D
250	1.33e−2	5.80e−3	1.36e−2
500	1.51e−1	8.73e−2	1.52e−1
1000	1.43	1.15	1.44
2000	13.1	12.3	13.1
3000	49.6	48.1	49.6

(c) Layup $L7$ varying the beam length

L(mm)	KLWI	KLWZ	3D
250	1.02e−2	5.42e−3	1.04e−2
500	1.17e−1	7.65e−2	1.17e−1
1000	1.02	0.85	1.03
2000	7.90	7.39	7.90
3000	26.9	25.9	26.9

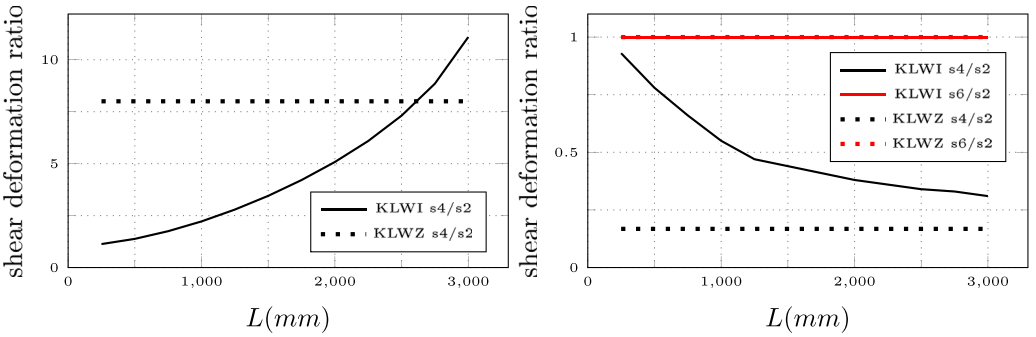

(a) Layup $L5_C$ (b) Layup $L7$

Fig. 7. Cantilever beam under transverse load: mean transverse shear deformation (s) ratio of the soft interlayers in the linear elastic solution varying the beam length. Layup $L5_C$ has two soft interlayers, denoted as 2 and 4 counting from the bottom. Layup $L7$ has three soft interlayers, denoted as 2, 4, 6 counting from the bottom, with 2 and 6 of uniform thickness and material.

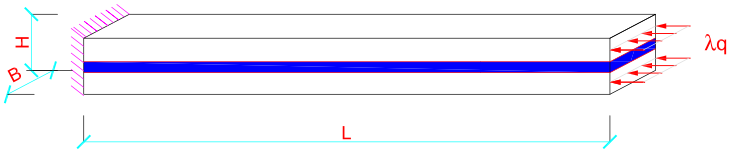

Fig. 8. Cantilever beam under compression: geometry, load, and boundary conditions.

curve of the imperfect structure for the two layups and the different models, in terms of load multiplier vs. transverse displacement at the free end. In this case, the coarsest mesh is sufficient for the KLWI model to capture the right behavior of the structure, in agreement with 3D solution. Instead, the basic KL model dramatically over-estimates the buckling load of the structure.

5.2. 3-Layer simply supported square plate

5.2.1. Large deflection under transverse load

The large deformation of a simply supported square plate under a transverse load is studied in this test. Geometry, load and boundary conditions are reported in Fig. 10. Both the layups $L3_A$ and $L3_B$ are considered in the test. The support is applied on the perimeter of the middle surface of the shell. The reference surface load is $q = 10^{-4}$ MPa for both the stacking sequences.

Different meshes are considered for the KLWI model, while only the finest mesh is adopted for the basic KL model. The reference shell surface corresponds to the middle surface of the packet. In Fig. 11, the equilibrium path in terms of load factor vs. the out-of-plane displacement at the center of the plate is shown. The membrane contribution to the overall stiffness grows with the deformation rate, causing the increase of the curve slope. Once again, the superposition of the curves obtained with the KLWI model for the different meshes and the curve obtained from 3D model testifies to the high level of accuracy achievable by the proposed solution. Equally accurate is the representation of the stress field, as depicted in Fig. 12, where the stress component σ_{11} is plotted over the

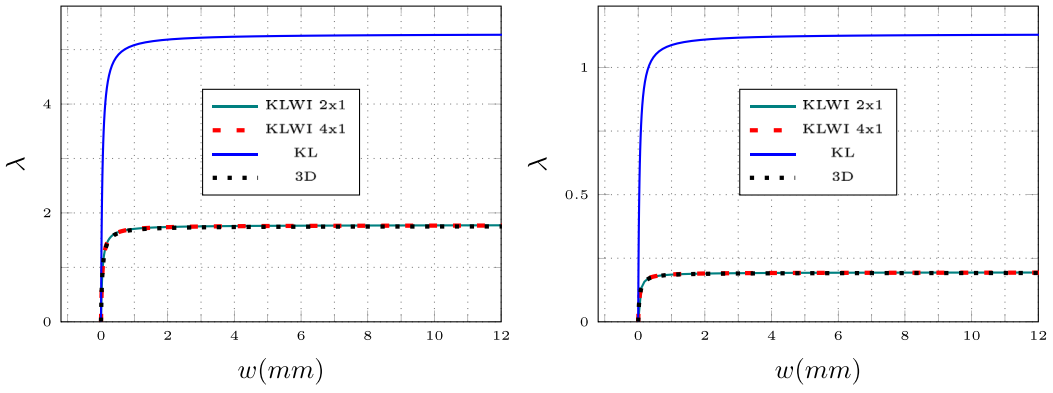

(a) Layup $L3_A$ (b) Layup $L3_B$

Fig. 9. Cantilever beam under compression: comparison of the equilibrium path in terms of vertical displacement component at the free end (w) obtained by KLWI, KL shell model and 3D model.

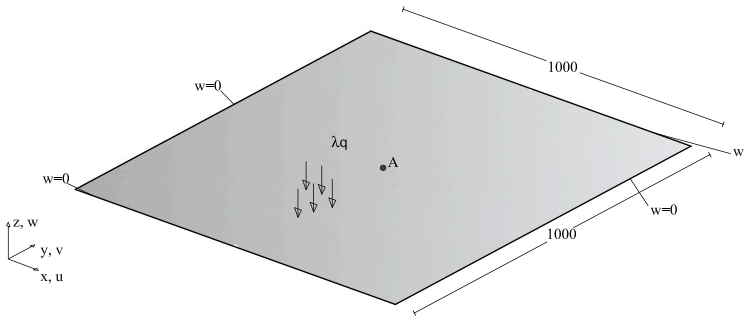

Fig. 10. 3-layer square plate under transverse load: geometry (mm), load and boundary conditions.

Table 3
3-layer square plate under transverse load: Number of total Newton–Raphson iterations and final displacement vs number of increments to reach the maximum load factor $\lambda = 3$ for layup $L3_B$ and shell model KLWI (coincident with KLWZ) with a mesh 16 × 16 and comparison with Abaqus 3D.

Load subdivisions	Total NR iterations KLWI	Total NR iterations KLWI (MIP)	$-w_A$ (mm) KLWI (MIP)	Total NR iterations Abaqus 3D
1	fails	7	14.2768	fails
2	23	11	14.2768	fails
4	27	16	14.2768	fails
20	70	47	14.2768	56

top and bottom surfaces of the glass layers for the different meshes. Also here, the correct representation of the results is achieved with coarse meshes and validated by the 3D solution. Similar conclusions are addressed for the evaluation of the shear strain γ_{13} in the interlayer, reported in Fig. 13. It is worth noting the accuracy of the proposed hierarchic model also when the strain of the interlayer is actually significant. The distribution of σ_{11} and γ_{13} along the thickness is also illustrated in Fig. 14 corresponding to their respective surface points of maximum.

Finally, the path-independence and the iterative performances of the numerical model are assessed in Table 3 for layup $L3_B$. To this aim, a load-controlled scheme with fixed step length is adopted here. The maximum load level is reached with an assigned number of load subdivisions (steps). When using a single load step, the standard full Newton is not able to converge to the equilibrium configuration. It can obtain the solution only by 2 or more load subdivisions and a relevant number of total iterations (linear systems). The significant nonlinearity of the problem is also confirmed by Abaqus 3D (Static general, full Newton, default settings), which requires as many as 20 load increments and 56 total iterations. Instead, the proposal with the MIP Newton scheme [40,41] is able to provide the solution with a single load step and only 7 total iterations. In any case, the predicted final displacement for the maximum load is exactly the same independently of the incrementation procedure highlighting the path-independence of the proposal.

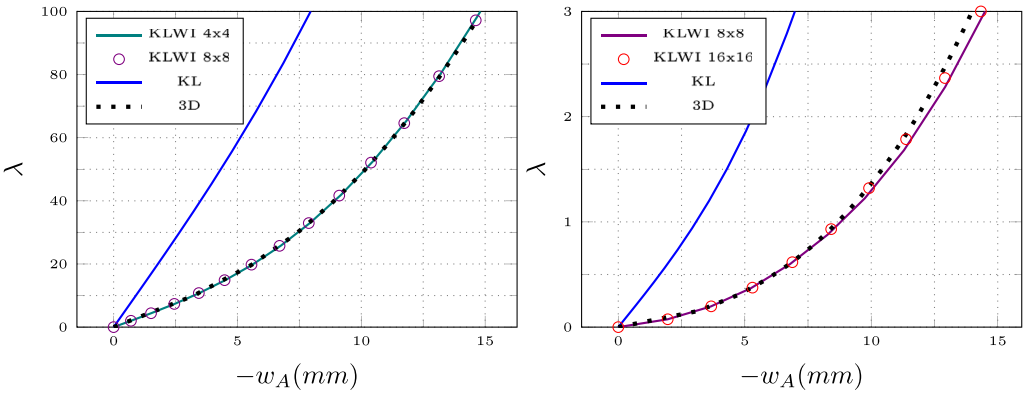

(a) Layup $L3_A$ (b) Layup $L3_B$

Fig. 11. 3-layer square plate under transverse load: equilibrium path in terms of the transverse displacement component at the plate center and comparison between KLWI shell model, KL shell model and the solid model from Abaqus.

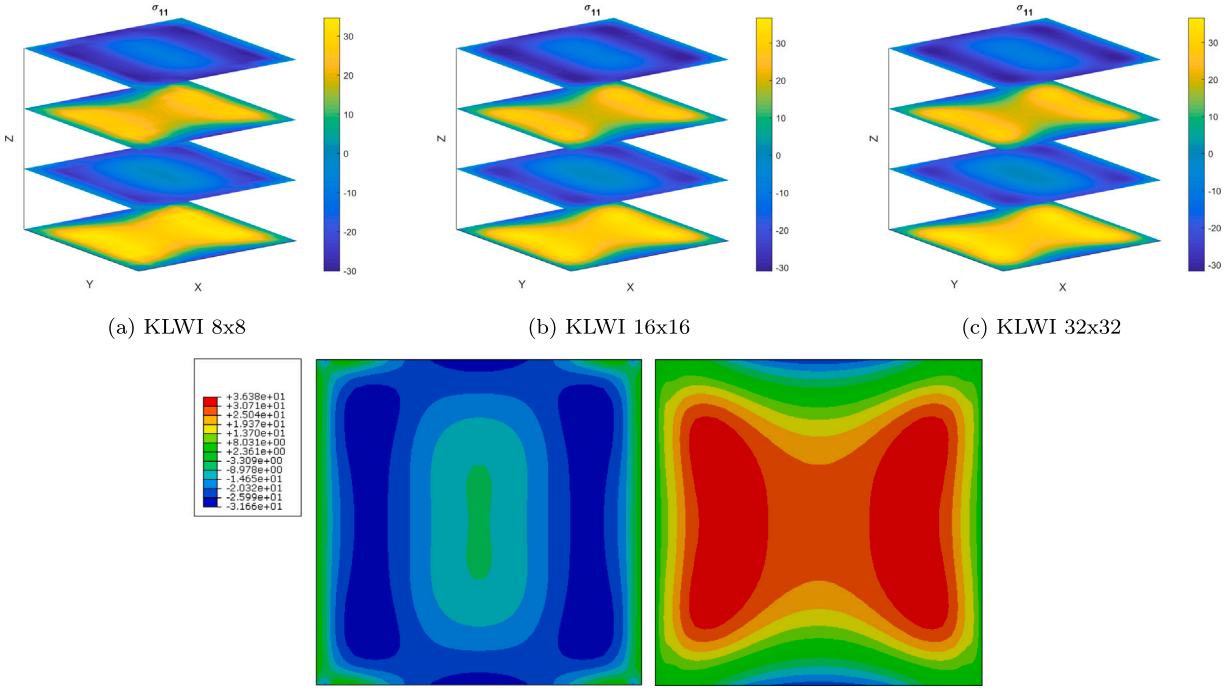

(a) KLWI 8x8 (b) KLWI 16x16 (c) KLWI 32x32

(d) Bottom (on the left) and top (on the right) laminate surfaces from 3D

Fig. 12. 3-layer square plate under transverse load: convergence of the stress component σ_{11} (MPa) at the last equilibrium point over the top and bottom surfaces of the stiff layers and comparison with 3D model for layup $L3_A$.

5.2.2. *Buckling under in-plane shear load*

The following test addresses the buckling behavior of a simply supported square plate under a self-equilibrated in-plane shear load. The $L3_A$ and $L3_B$ stacking sequences are analyzed. Geometry, loads and boundary conditions are illustrated in Fig. 15. The reference edge compression load is $q = h_{st} \cdot 1$ MPa, with h_{st} (mm) the sum of the thicknesses of the stiff layers, in the direction parallel to each edge. The support is applied on the perimeter of the middle surface assumed as reference shell surface.

The plate is discretized with progressively refining meshes for the KLWI model, while, as in the previous tests, only the finest mesh is used for the basic KL model. A geometric imperfection with the shape of the first linearized buckling mode and an amplitude equal to 0.1 mm is added to the perfect model. The equilibrium path of the imperfect structure is shown in Fig. 16 in terms of out-of-plane displacement of the plate center and the buckling modes are depicted right below the curves for both the layups. The imperfection causes a smooth change in the behavior and the stiffness reduction after the buckling point. Also in this case the KLWI model proves

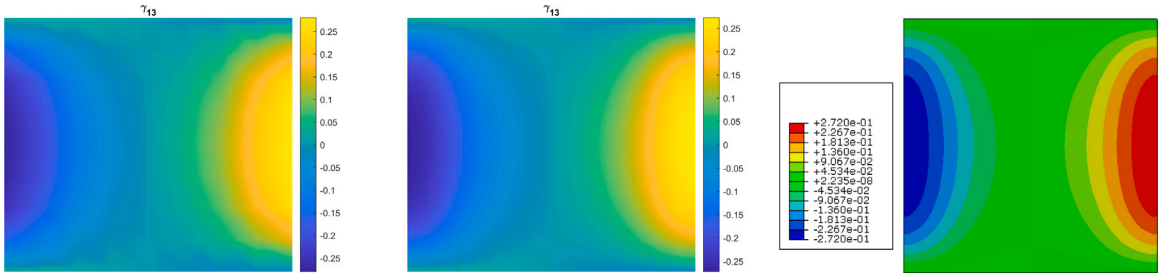

(a) KLWI 8x8 (b) KLWI 16x16 (c) 3D

Fig. 13. 3-layer square plate under transverse load: convergence of the transverse shear strain γ_{13} over the interlayer and comparison to 3D model results from Abaqus for layup $L3_A$ at the last equilibrium point.

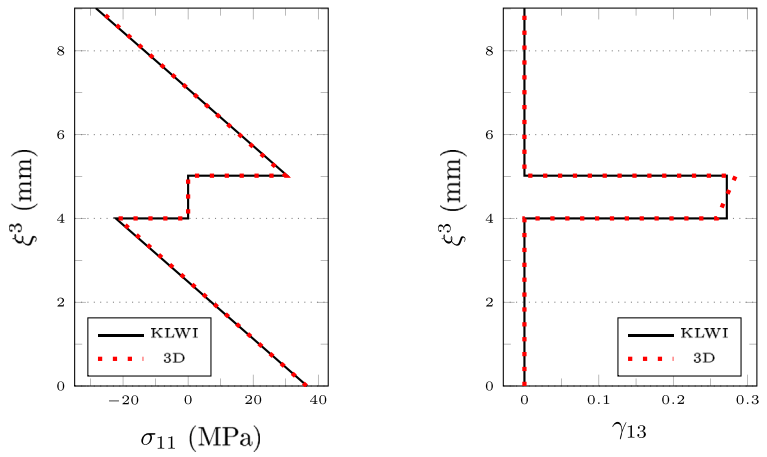

Fig. 14. 3-layer square plate under transverse load: through-the-thickness distribution of σ_{11} (MPa) and γ_{13} at the last equilibrium point at the their peak point for layup $L3_A$ and comparison to 3D Abaqus model.

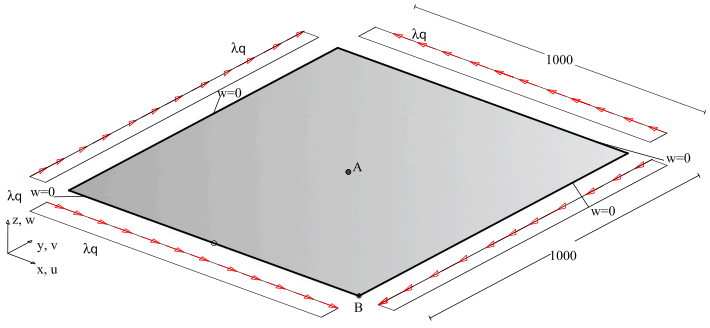

Fig. 15. 3-layer square plate under transverse load: geometry (mm), load and boundary conditions.

to be accurate, if compared to the reference 3D solution. Similarly, the stress field is well represented with coarse meshes, as can be seen in Figs. 17 where the component σ_{11} is shown for $L3_A$ and for the different meshes adopted. The corresponding values obtained by the 3D model are reported for comparison. Finally, the coarse-mesh accuracy of the results is confirmed also for the transverse shear strain γ_{13} in the interlayer, as reported in Figs. 18 and 19 for the two layups. It is worth noting that $L3_B$ generally requires a little finer mesh compared to $L3_A$. From the strain plots, it is clear that this is not due to some sort of locking, but just to the narrower bands characterizing the $L3_B$ solution.

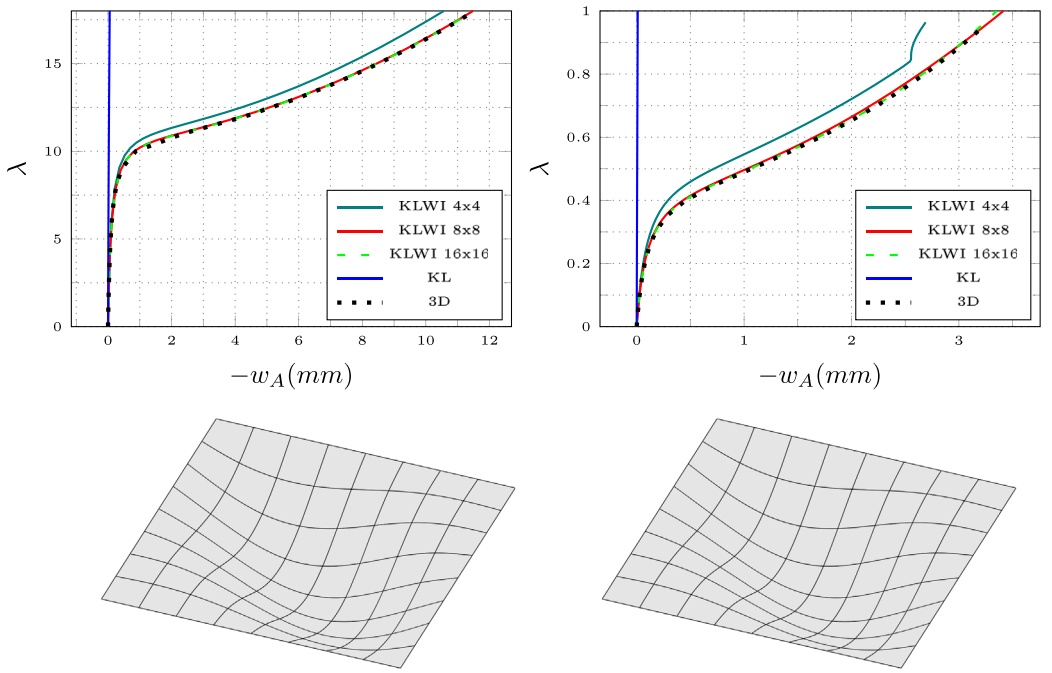

(a) layup $L3_A$ (b) layup $L3_B$

Fig. 16. 3-layer square plate under in-plane shear: equilibrium path in terms of the transverse displacement component at the plate center obtained by KLWI and KL shell model and 3D model with illustration of the first linearized buckling mode for the two layups.

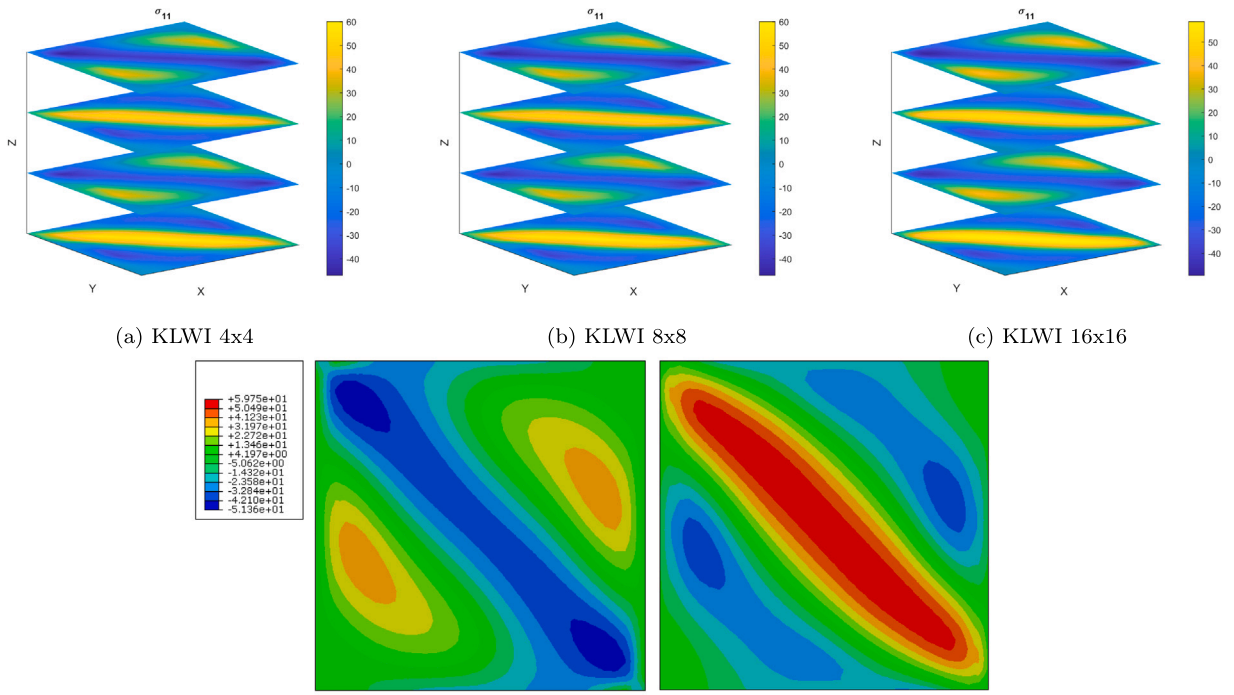

(a) KLWI 4x4 (b) KLWI 8x8 (c) KLWI 16x16

(d) Top (on the left) and bottom (on the right) laminate surfaces from 3D

Fig. 17. 3-layer square plate under in-plane shear: convergence of the stress component σ_{11} (MPa) at the last equilibrium point over the top and bottom surfaces of the stiff layers and comparison with 3D model for layup $L3_A$.

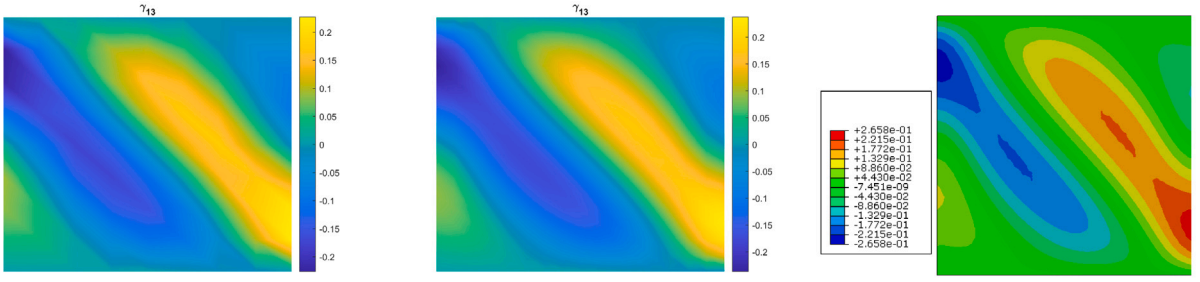

(a) KLWI 8x8 (b) KLWI 16x16 (c) 3D

Fig. 18. 3-layer square plate under in-plane shear: convergence of transverse shear strain γ_{13} at the last equilibrium point over the interlayer and comparison to solid model results from Abaqus for layup $L3_A$.

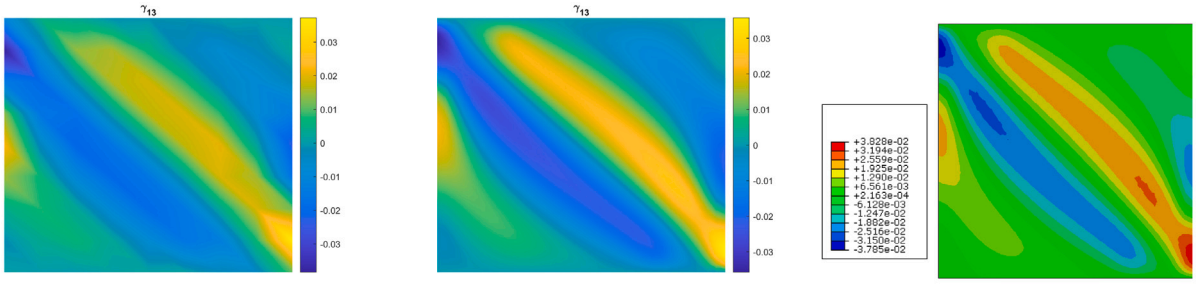

(a) KLWI 8x8 (b) KLWI 32x32 (c) 3D

Fig. 19. 3-layer square plate under in-plane shear: convergence of the transverse shear strain γ_{13} over the interlayer and comparison to solid model results from Abaqus for layup $L3_B$ at the last equilibrium point.

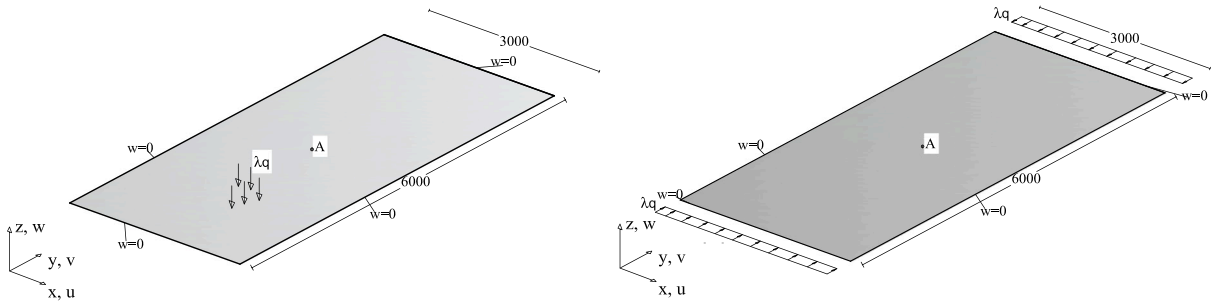

(a) Transverse load (b) Axial compression

Fig. 20. Rectangular plate: geometry (mm), loads, and boundary conditions.

5.3. 5-Layer rectangular plate simply supported on 4 edges

The following test aims at analyzing the performance of the proposed model in case of more than 3 layers. A rectangular simply supported plate made of 5 alternating layers (layup $L5$) is considered for this purpose. The support is assigned on the perimeter of the bottom layer. Two different loading cases are assumed:

- Transverse load $q = 10^{-3}$ MPa distributed over the top layer;
- Axial compression edge load $q = h_{st} \cdot 1$ MPa, with h_{st} (mm) the sum of the thicknesses of the stiff layers, distributed along the short edges.

Geometry, loads and boundary conditions are depicted in Fig. 20. The analysis is carried out for different meshes, with double number of elements over the longer edges, for the layup $L5_A$ (symmetric and with uniform soft layers). The equilibrium paths are

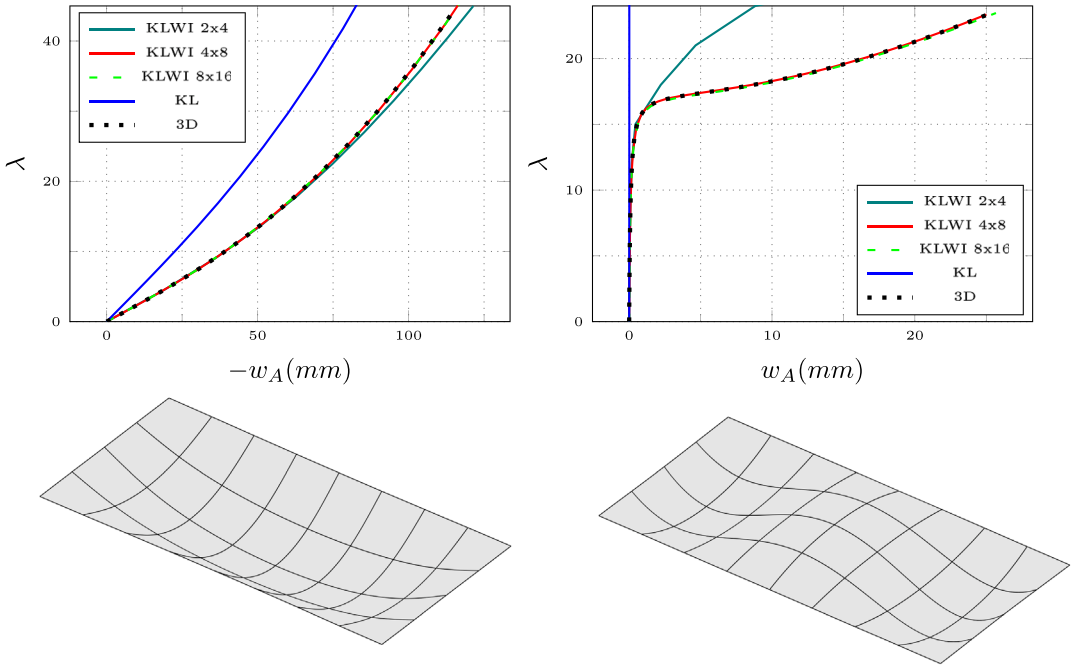

(a) Transverse load (b) Axial compression

Fig. 21. 5-layer rectangular plate: equilibrium path in terms of the transverse displacement component at the plate center for KLWI shell model, KL shell model and 3D model for the two load cases and layup $L5_A$. Deformed configuration plots for the maximum load factor (scale factor 10).

Table 4
5-layer rectangular plate under compression load: Linearized buckling load multiplier for the different models and layups.

Layup	KL	KLWI	KLWZ	3D
$L5_A$	43.40	17.42	17.42	17.43
$L5_B$	14.59	8.045	8.055	8.050
$L5_C$	44.94	11.24	14.15	11.53

plotted in Fig. 21. The two load conditions are characterized by large deflection and buckling respectively. In particular, for the second load case, the structure is nudged on the bifurcated path introducing a geometric imperfection with the shape of the first linearized buckling mode and a maximum deviation equal to 0.1 mm. The deformed configurations at the last equilibrium point are also reported below the curves in Fig. 21. The comparisons of the different models confirms the accuracy of the proposed KLWI model also in case of multiple soft layers, unlike the basic KL model. Also in this case, coarse meshes are sufficient to obtained the solid reference solution. The analysis is repeated for a fine converged mesh also for the other 5-layer layups: $L5_B$ (non-uniform stiff layers and uniform soft layers) and $L5_C$ (uniform stiff layers and non-uniform soft layers). The corresponding load–deflection curves are depicted in Fig. 22 for the transverse load case, including the comparison with the model with a single zigzag warping function KLWZ. It is possible to observe that, also in this case, KLWZ proves to be a convenient alternative (fewer DOFs) to KLWI for alternating layups with uniform soft layers, while it results less accurate for non-uniform soft layers. Similar considerations hold when considering the compression load case, for which the linearized buckling load multiplier is reported in Table 4 for the different models and layups. KLWZ has the same accuracy as KLWI for $L5_A$ and $L5_B$, while the non-uniform soft layers of $L5_C$ negatively affects its prediction. On the other hand, considering the geometry of $L5_A$, Fig. 23 demonstrates the reliability of KLWZ for uniform soft layers in predicting the linearized buckling load also for all possible stiffness ratio of the two materials. Interestingly, when the stiffness of the soft layers tends to vanish, the hierarchic model is able to recover the correct limit P_{crit0} of the uncoupled stiff layers. Furthermore, the basic KL gets inaccurate for stiffness ratios $E_{soft}/E_{stiff} < 10^{-2}$.

5.4. Curved panel under vertical load

The final test concerns the nonlinear analysis of the curved laminated glass panel whose geometry and boundary condition are reported in Fig. 24. The aim of the test is just to assess the correctness of the hierarchic formulation for initially curved geometries.

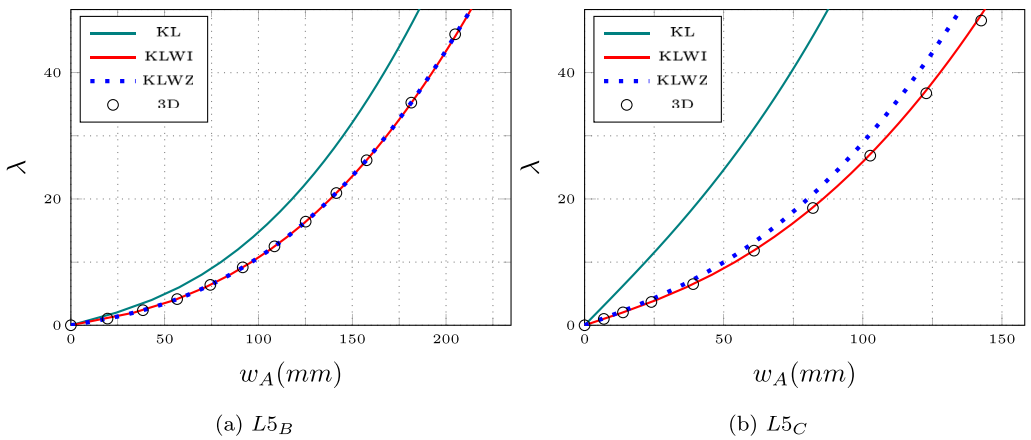

Fig. 22. 5-layer rectangular plate under transverse load: converged equilibrium path in terms of the transverse displacement component at the plate center for KLWI shell model, KL shell model and 3D model for layup $L5_B$ and $L5_C$.

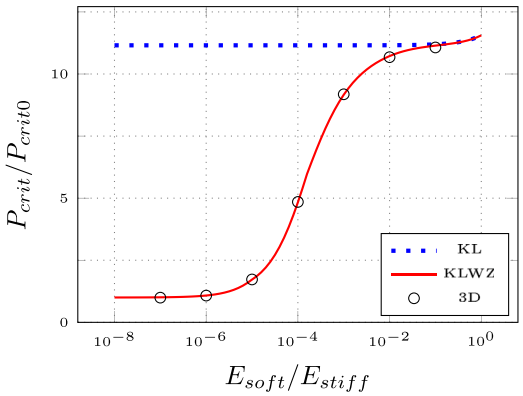

Fig. 23. 5-layer rectangular plate under compression load: linearized buckling load multiplier for layup $L5_A$ normalized with respect to that of the uncoupled stiff layers P_{crit0} varying the stiffness ratio of the layers.

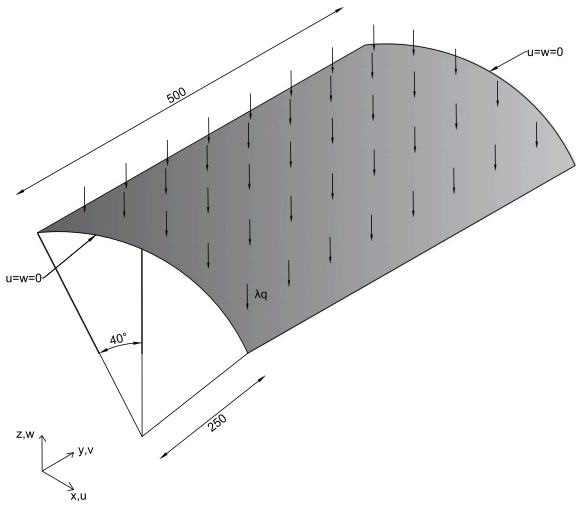

Fig. 24. Curved panel: geometry (mm), loads, and boundary conditions.

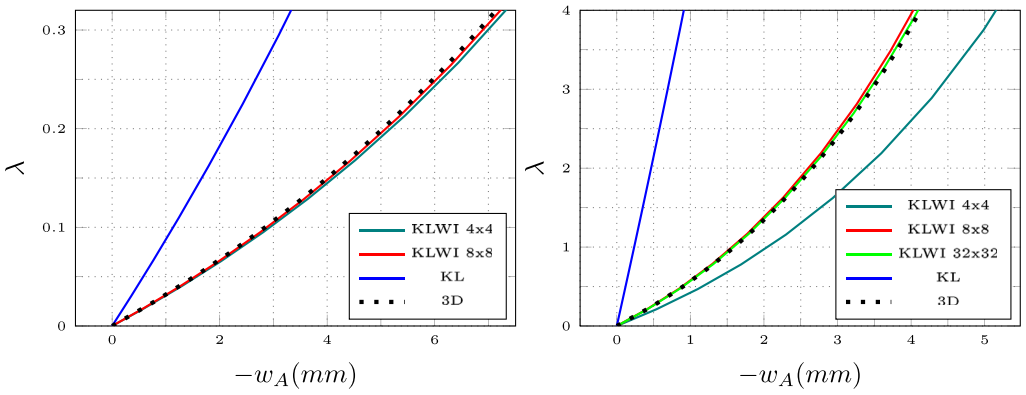

(a) Layup $L3_A$ (b) Layup $L3_B$

Fig. 25. Curved panel: equilibrium path in terms of the transverse displacement component at the mid point of the longitudinal edge and comparison of KLWI shell model, KL shell model and 3D results.

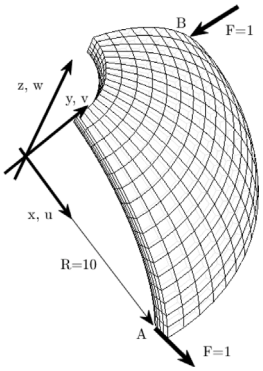

Fig. 26. Hemispherical shell: geometry (enlarged in the thickness direction) and applied loads.

A vertical distributed load $q = 1$ MPa and $q = 10^{-3}$ MPa are applied for the layup $L3_A$ and $L3_B$ respectively. The roof is modeled using four different meshes, varying the number of elements in both dimensions from 4 to 32, each time doubling the refinement. In Fig. 25 the vertical displacement at the midpoint of the straight side of the structure is reported against the load multiplier λ. The KLWI model is compared to the KL model and the reference prediction obtained using the solid model in Abaqus. The reference shell surface corresponds to the lower surface of the laminate where the support is applied. The results testify the accuracy of the proposed model also in the case of curved geometries. The remarkable coarse-mesh accuracy of the discretization method is confirmed also in this case.

5.5. Multi-layer hemispherical shell with 18° cut-off

This benchmark concerns a 5-layer hemispherical shell with a circular cut-off at its top, as reported in Fig. 26 (one quarter of the shell with symmetric boundary conditions), with the same geometry, loads and material layups proposed in [22]. The input data are given in dimensionless form as in [22]. The hole aperture is 18°, the sphere radius is 10, and the shell thickness is $h = 0.075$. The shell is subjected to equal and opposite concentrated forces applied at the 4 cardinal points of its equator amplified by the factor λ. The top and bottom curved edges are free. The rigid body motion is eliminated by fixing the vertical displacement at an arbitrary point. This final tests is aimed at assessing the accuracy of the proposed shell models for a doubly curved shell and for very large deformations. Three alternative layups are considered, including symmetric and asymmetric laminations. The layer material type and thickness for each layup are reported in Table 5, where layer 1 denotes the interior layer of the hemispherical shell. The material parameters for the stiff layers (F) and soft layers (C) are: $E_F = 1.0 \times 10^7$, $E_C = 5.0 \times 10^3$ and $\nu_F = \nu_C = 0.2$.

Exploiting the symmetry, only one quarter of the shell is modeled. The nonlinear load–displacement curves (see Fig. 27) obtained with the proposals are in good agreement with those reported in [22] and obtained with a Reissner corotational shell model enhanced with warping which reproduces the 3D solution. As observed for the other tests, KLWZ gives the correct solution (coincident with KLZI) for layups $HL1$ and $HL3$ characterized by uniform soft layers (same thickness and material), while a small error affects the solution for $HL2$. This error is smaller in this test compared to the others due to the milder difference in the stiffness of the materials

Table 5
Hemispherical shell: Description of the three layups, labeled as $HL1$, $HL2$ and $HL3$.

Layer index	Layer material	Layer thickness		
		$HL1$	$HL2$	$HL3$
1	(F)	1/5h	1/15h	3/25h
2	(C)	1/5h	2/15h	5/25h
3	(F)	1/5h	3/15h	9/25h
4	(C)	1/5h	4/15h	5/25h
5	(F)	1/5h	5/15h	3/25h

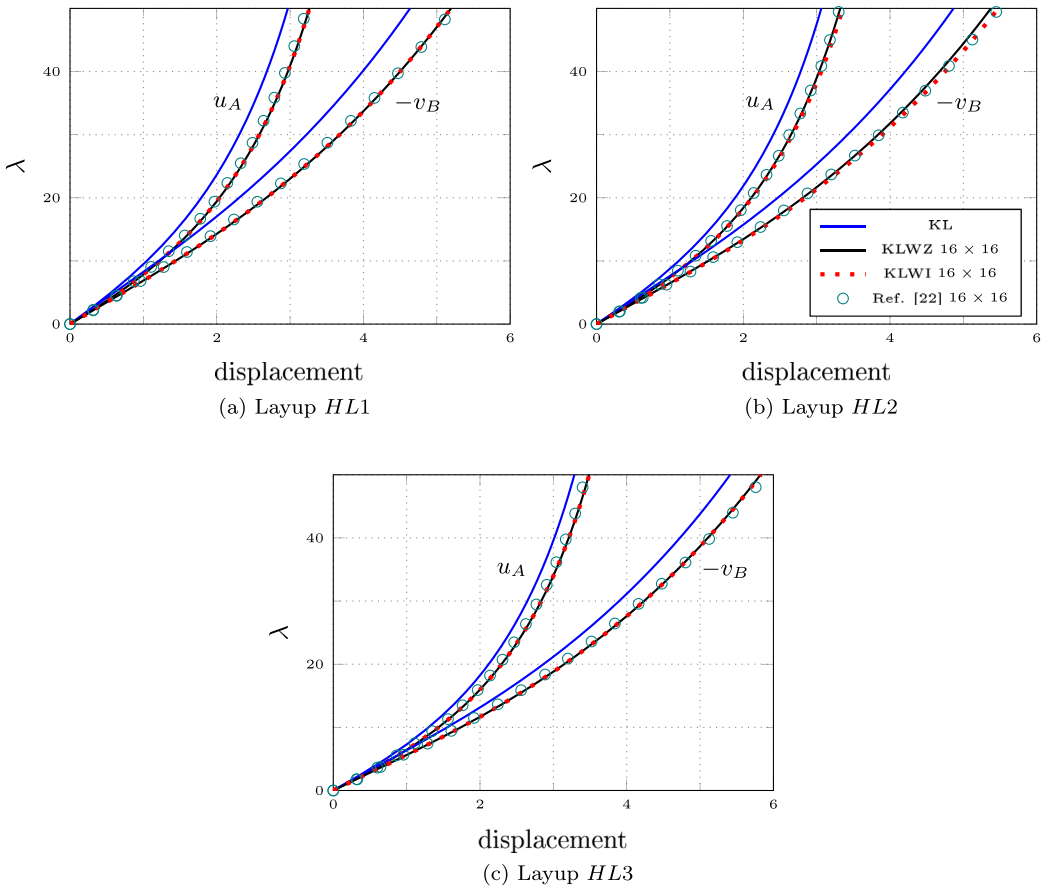

(a) Layup $HL1$ (b) Layup $HL2$

(c) Layup $HL3$

Fig. 27. Equilibrium paths for the hemispherical shell: comparison of KLWZ and KLWI shell models with the results from [22] for layup $HL1$, $HL2$ and $HL3$.

and is canceled when using KLWI. This confirms the reliability of our more efficient models with warping (fewer DOFs compared to [22]) also for doubly curved shells undergoing very large displacements (more than half the radius) and rotations. As shown in [22], the FSDT shell is inaccurate in this case due to the significant warping, with results close to the KL solution reported in Fig. 27.

Efficiency and robustness of the nonlinear solver are also investigated in Table 6. The maximum load is reached in an assigned number of load increments for $HL3$, that is the most flexible layup. Abaqus 3D (Static general, full Newton, default settings) requires as many as 20 load increments and 83 total iterations to complete the analysis. The proposal KLWZ with the adopted MIP implementation of the Newton method is able to compute in a single load step and only 5 iterations the final deformed configuration for the maximum load with displacements of about 0.6 of the initial radius.

6. Conclusions

This work presented a Total Lagrangian large deformation Kirchhoff–Love model hierarchically enhanced with warping profiles generically selected by the user. The small strain hypothesis was exploited to derive a simple and efficient yet accurate strain

Table 6
Hemispherical shell: Number of total Newton–Raphson iterations vs number of increments to reach the maximum load factor $\lambda = 50$ for layup $HL3$ using the shell model KLWZ (coincident with KLWI) with a mesh 16×16 and Abaqus 3D.

Load subdivisions	Total NR iterations KLWZ (MIP)	Total NR iterations Abaqus 3D
1	5	Fails
5	16	Fails
10	29	Fails
20	47	83

measure. An effective NURBS-based discretization was proposed for the problem in weak form, characterized by excellent coarse-mesh accuracy and small number of integration points. A numerical investigation demonstrated the correctness of the hierarchic formulation in large displacement and buckling problems. Particular attention was given to the modeling of alternating stiff/soft stacking sequences, representing a technically significant example characterized by a peculiar warping profile: transverse shear strains concentrate in the soft interlayers while the stiff layers behave as Kirchhoff–Love shells with equal rotation of the normal. Two warping models were studied: (1) independent transverse shear deformations of the soft layers and (2) single zigzag function linking these deformations. The comparison with the reference solid solution showed the great accuracy and reliability of the first warping model, whose number of DOFs depends on the number of soft layers, when usual shell models provide largely wrong predictions. On the other hand, the second warping model allows to reduce the unknowns to five per surface point regardless of the number of layers. This reduction produces no loss of accuracy when the soft interlayers are uniform in terms of thickness and stiffness, as in most practical cases. However, the first warping model is recommended for non-uniform soft layers. In this case, the actual warping profile varies widely even with structural properties other than the layup, so that a single zigzag function, whatever it is, results unreliable. The first warping model seems also the ideal choice for more complex simulations taking into account also thermal and viscous effects.

Declaration of competing interest

The authors declare that they have no known competing financial interests or personal relationships that could have appeared to influence the work reported in this paper.

Data availability

The data is reported in the paper.

References

[1] P. Lenk, H. Lambert, Practical aspects of finite-element analysis in structural glass design, Proc. Inst. Civ. Eng. 168 (7) (2015) 527–538, http://dx.doi.org/10.1680/stbu.13.00104.
[2] J. Kiendl, K.-U. Bletzinger, J. Linhard, R. Wuchner, Isogeometric shell analysis with Kirchhoff–Love elements, Comput. Methods Appl. Mech. Engrg. 198 (49) (2009) 3902–3914, http://dx.doi.org/10.1016/j.cma.2009.08.013, URL https://www.sciencedirect.com/science/article/pii/S0045782509002680.
[3] L. Leonetti, D. Magisano, A. Madeo, G. Garcea, J. Kiendl, A. Reali, A simplified Kirchhoff–Love large deformation model for elastic shells and its effective isogeometric formulation, Comput. Methods Appl. Mech. Engrg. 354 (2019) 369–396, http://dx.doi.org/10.1016/j.cma.2019.05.025.
[4] A. Patton, P. Antolin, J.-E. Dufour, J. Kiendl, A. Reali, Accurate equilibrium-based interlaminar stress recovery for isogeometric laminated composite Kirchhoff plates, Compos. Struct. 256 (2021) 112976, http://dx.doi.org/10.1016/j.compstruct.2020.112976.
[5] M.L. Sanchez, P.M. Pimenta, A. Ibrahimbegovic, A simple geometrically exact finite element for thin shells-Part 1: statics, Comput. Mech. (2023) http://dx.doi.org/10.1007/s00466-023-02339-2.
[6] J. Reddy, On refined theories of composite laminates, Meccanica 25 (1990) 230–238.
[7] F. Gruttmann, W. Wagner, An advanced shell model for the analysis of geometrical and material nonlinear shells, Comput. Mech. 66 (6) (2020) 1353–1376, http://dx.doi.org/10.1007/s00466-020-01905-2.
[8] Y. Cho, R. Averill, First-order zig-zag sublaminate plate theory and finite element model for laminated composite and sandwich panels, Compos. Struct. 50 (1) (2000) 1–15, http://dx.doi.org/10.1016/S0263-8223(99)00063-X.
[9] E. Carrera, Historical review of Zig-Zag theories for multilayered plates and shells, Appl. Mech. Rev. 56 (3) (2003) 287–308, http://dx.doi.org/10.1115/1.1557614.
[10] L. Demasi, Refined multilayered plate elements based on murakami zig-zag functions, Compos. Struct. 70 (3) (2005) 308–316, http://dx.doi.org/10.1016/j.compstruct.2004.08.036.
[11] M. Gherlone, A. Tessler, M.D. Sciuva, C0 beam elements based on the refined zigzag theory for multilayered composite and sandwich laminates, Compos. Struct. 93 (11) (2011) 2882–2894, http://dx.doi.org/10.1016/j.compstruct.2011.05.015.
[12] A. Eijo, E. Onate, S. Oller, A four-noded quadrilateral element for composite laminated plates/shells using the refined zigzag theory, Internat. J. Numer. Methods Engrg. 95 (8) (2013) 631–660, http://dx.doi.org/10.1002/nme.4503.
[13] L. Iurlaro, M. Gherlone, M. Di Sciuva, A. Tessler, Assessment of the refined zigzag theory for bending, vibration, and buckling of sandwich plates: a comparative study of different theories, Compos. Struct. 106 (2013) 777–792, http://dx.doi.org/10.1016/j.compstruct.2013.07.019.
[14] J. Reddy, Mechanics of Laminated Composite Plates and Shells: Theory and Analysis, second ed., CRC Press, 2003, http://dx.doi.org/10.1201/b12409.
[15] A. Ferreira, G. Fasshauer, R. Batra, J. Rodrigues, Static deformations and vibration analysis of composite and sandwich plates using a layerwise theory and rbf-ps discretizations with optimal shape parameter, Compos. Struct. 86 (4) (2008) 328–343, http://dx.doi.org/10.1016/j.compstruct.2008.07.025.

[16] C.H. Thai, A. Ferreira, E. Carrera, H. Nguyen-Xuan, Isogeometric analysis of laminated composite and sandwich plates using a layerwise deformation theory, Compos. Struct. 104 (2013) 196–214, http://dx.doi.org/10.1016/j.compstruct.2013.04.002.
[17] Y. Guo, M. Ruess, A layerwise isogeometric approach for nurbs-derived laminate composite shells, Compos. Struct. 124 (2015) 300–309, http://dx.doi.org/10.1016/j.compstruct.2015.01.012.
[18] Y. Bazilevs, M.S. Pigazzini, A. Ellison, H. Kim, A new multi-layer approach for progressive damage simulation in composite laminates based on isogeometric analysis and Kirchhoff–Love shells. Part I: basic theory and modeling of delamination and transverse shear, Comput. Mech. 62 (2018) 563–585, http://dx.doi.org/10.1007/s00466-017-1513-1.
[19] M. Pigazzini, D. Kamensky, D. van Iersel, M. Alaydin, J. Remmers, Y. Bazilevs, Gradient-enhanced damage modeling in Kirchhoff–Love shells: Application to isogeometric analysis of composite laminates, Comput. Methods Appl. Mech. Engrg. 346 (2019) 152–179, http://dx.doi.org/10.1016/j.cma.2018.10.042, URL https://www.sciencedirect.com/science/article/pii/S0045782518305462.
[20] M. Alaydin, M. Behzadinasab, Y. Bazilevs, Isogeometric analysis of multilayer composite shell structures: Plasticity, damage, delamination and impact modeling, Int. J. Solids Struct. 252 (2022) 111782, http://dx.doi.org/10.1016/j.ijsolstr.2022.111782, URL https://www.sciencedirect.com/science/article/pii/S0020768322002736.
[21] F.G. Flores, Implementation of the refined zigzag theory in shell elements with large displacements and rotations, Compos. Struct. 118 (2014) 560–570, http://dx.doi.org/10.1016/j.compstruct.2014.07.034.
[22] Y. Liang, B. Izzuddin, Nonlinear analysis of laminated shells with alternating stiff/soft lay-up, Compos. Struct. 133 (2015) 1220–1236, http://dx.doi.org/10.1016/j.compstruct.2015.08.043.
[23] K. Sze, W. Chan, T. Pian, An eight-node hybrid-stress solid-shell element for geometric non-linear analysis of elastic shells, Internat. J. Numer. Methods Engrg. 55 (7) (2002) 853–878, http://dx.doi.org/10.1002/nme.535.
[24] M. Schwarze, S. Reese, A reduced integration solid-shell finite element based on the EAS and the ANS concept-large deformation problems, Internat. J. Numer. Methods Engrg. 85 (3) (2011) 289–329, http://dx.doi.org/10.1002/nme.2966.
[25] L. Leonetti, F. Liguori, D. Magisano, G. Garcea, An efficient isogeometric solid-shell formulation for geometrically nonlinear analysis of elastic shells, Comput. Methods Appl. Mech. Engrg. 331 (2018) 159–183, http://dx.doi.org/10.1016/j.cma.2017.11.025.
[26] P.M. Pinsky, K.O. Kim, A multi-director formulation for nonlinear elastic-viscoelastic layered shells, Comput. Struct. 24 (6) (1986) 901–913, http://dx.doi.org/10.1016/0045-7949(86)90298-1, URL https://www.sciencedirect.com/science/article/pii/0045794986902981.
[27] W.B. Kratzig, D. Jun, Multi-layer multi-director concepts for D-adaptivity in shell theory, Comput. Struct. 80 (9) (2002) 719–734, http://dx.doi.org/10.1016/S0045-7949(02)00043-3, URL https://www.sciencedirect.com/science/article/pii/S0045794902000433.
[28] L. Galuppi, G. Royer-Carfagni, Shear coupling effects of the core in curved sandwich beams, Composites B 76 (2015) 320–331, http://dx.doi.org/10.1016/j.compositesb.2015.01.045.
[29] H.S. Norville, K.W. King, J.L. Swofford, Behavior and strength of laminated glass, J. Eng. Mech. 124 (1) (1998) 46–53, http://dx.doi.org/10.1061/(ASCE)0733-9399(1998)124:1(46).
[30] I.V. Ivanov, D.S. Velchev, N.G. Georgiev, I.D. Ivanov, T. Sadowski, A plate finite element for modelling of triplex laminated glass and comparison with other computational models, Meccanica 51 (2016) 341–358, http://dx.doi.org/10.1007/s11012-015-0275-0.
[31] C. Felippa, B. Haugen, A unified formulation of small-strain corotational finite elements: I. theory, Comput. Methods Appl. Mech. Eng. 194 (21) (2005) 2285–2335, http://dx.doi.org/10.1016/j.cma.2004.07.035.
[32] Y. Liang, F. Lancaster, B. Izzuddin, Effective modelling of structural glass with laminated shell elements, Compos. Struct. 156 (2016) 47–62, http://dx.doi.org/10.1016/j.compstruct.2016.02.077, 70th Anniversary of Professor J. N. Reddy.
[33] J. Simo, D. Fox, On a stress resultant geometrically exact shell model. part i: Formulation and optimal parametrization, Comput. Methods Appl. Mech. Engrg. 72 (3) (1989) 267–304, http://dx.doi.org/10.1016/0045-7825(89)90002-9.
[34] B. Oesterle, R. Sachse, E. Ramm, M. Bischoff, Hierarchic isogeometric large rotation shell elements including linearized transverse shear parametrization, Comput. Methods Appl. Mech. Engrg. 321 (2017) 383–405.
[35] A.J. Herrema, E.L. Johnson, D. Proserpio, M.C. Wu, J. Kiendl, M.-C. Hsu, Penalty coupling of non-matching isogeometric Kirchhoff–Love shell patches with application to composite wind turbine blades, Comput. Methods Appl. Mech. Engrg. 346 (2019) 810–840, http://dx.doi.org/10.1016/j.cma.2018.08.038.
[36] A. Tessler, M.D. Sciuva, M. Gherlone, A refined zigzag beam theory for composite and sandwich beams, J. Compos. Mater. 43 (9) (2009) 1051–1081, http://dx.doi.org/10.1177/0021998308097730.
[37] A. Haydar, G. Royer-Carfagni, A simple model for inflexed multilayered laminated glass beams based on refined zig-zag theory, J. Appl. Mech. 90 (1) (2022) 011002, http://dx.doi.org/10.1115/1.4055810.
[38] T. Hughes, J. Cottrell, Y. Bazilevs, Isogeometric analysis: cad, finite elements, nurbs, exact geometry and mesh refinement, Comput. Methods Appl. Mech. Engrg. 194 (39) (2005) 4135–4195, http://dx.doi.org/10.1016/j.cma.2004.10.008.
[39] E. Riks, An incremental approach to the solution of snapping and buckling problems, Int. J. Solids Struct. 15 (7) (1979) 529–551, http://dx.doi.org/10.1016/0020-7683(79)90081-7.
[40] D. Magisano, L. Leonetti, G. Garcea, How to improve efficiency and robustness of the Newton method in geometrically non-linear structural problem discretized via displacement-based finite elements, Comput. Methods Appl. Mech. Engrg. 313 (2017) 986–1005, http://dx.doi.org/10.1016/j.cma.2016.10.023.
[41] D. Magisano, A. Corrado, New robust and efficient global iterations for large deformation finite element analysis of beams and shells with material nonlinearity, Comput. Methods Appl. Mech. Engrg. 406 (2023) 115900, http://dx.doi.org/10.1016/j.cma.2023.115900.
[42] D. Magisano, L. Leonetti, A. Madeo, G. Garcea, A large rotation finite element analysis of 3D beams by incremental rotation vector and exact strain measure with all the desirable features, Comput. Methods Appl. Mech. Engrg. 361 (2020) 112811, http://dx.doi.org/10.1016/j.cma.2019.112811.
[43] R. Pfefferkorn, S. Bieber, B. Oesterle, M. Bischoff, P. Betsch, Improving efficiency and robustness of enhanced assumed strain elements for nonlinear problems, Internat. J. Numer. Methods Engrg. 122 (8) (2021) 1911–1939, http://dx.doi.org/10.1002/nme.6605.
[44] W. Wagner, F. Gruttmann, A robust non-linear mixed hybrid quadrilateral shell element, Internat. J. Numer. Methods Engrg. 64 (5) (2005) 635–666, http://dx.doi.org/10.1002/nme.1387, URL https://onlinelibrary.wiley.com/doi/abs/10.1002/nme.1387.
[45] C. Adam, T. Hughes, S. Bouabdallah, M. Zarroug, H. Maitournam, Selective and reduced numerical integrations for NURBS-based isogeometric analysis, Comput. Methods Appl. Mech. Engrg. 284 (2015) 732–761, http://dx.doi.org/10.1016/j.cma.2014.11.001.
[46] K.A. Johannessen, Optimal quadrature for univariate and tensor product splines, Comput. Methods Appl. Mech. Engrg. 316 (2017) 84–99, http://dx.doi.org/10.1016/j.cma.2016.04.030, special Issue on Isogeometric Analysis: Progress and Challenges.